Human liver organoids; a patient-derived primary model for HBV Infection and Related Hepatocellular Carcinoma

Authors: Elisa De Crignis[1], Shahla Romal[1], Fabrizia Carofiglio[1], Panagiotis Moulos[2], Monique M.A. Verstegen[3], Mir Mubashir Khalid[1], Farzin Pourfarzad[4], Shringar Rao[1], Ameneh Bazrafshan[1], Christina Koutsothanassis[5], Helmuth Gehart[6], Tsung Wai Kan[1], Robert-Jan Palstra[1], Charles Boucher[7], Jan M.N. IJzermans[3], Meritxell Huch[8], Sylvia F. Boj[4], Robert Vries[4], Hans Clevers[6], Luc van der Laan[3], Pantelis Hatzis[2], Tokameh Mahmoudi[1*]

Affiliations:

[1] Department of Biochemistry, Erasmus University Medical Center, Ee634 PO Box 2040 3000CA Rotterdam, the Netherlands

[2] Biomedical Sciences Research Center 'Alexander Fleming', 16672 Vari, Greece

[3] Department of Surgery, Erasmus University Medical Center, PO Box 2040 3000CA Rotterdam, the Netherlands

[4] Foundation Hubrecht Organoid Technology (HUB), 3584 CT Utrecht, the Netherlands

[5] HybridStat Predictive Analytics, 34 Panos Street, 16672 Vari, Greece

[6] Hubrecht Institute-KNAW, University Medical Centre Utrecht, CancerGenomics.nl, Uppsalalaan 8, 3584 CM Utrecht, the Netherlands

[7] Department of Viroscience, Erasmus Medical Centre, Rotterdam, the Netherlands

[8] Wellcome Trust/Cancer Research UK University of Cambridge. Tennis court Road, CB2 1QN, Cambridge United Kingdom

[*] Correspondence to: Tokameh Mahmoudi: t.mahmoudi@erasmusmc.nl, Phone N: +31 (0)107043331, Fax N: +31(0)10704747

Abstract The molecular events that drive Hepatitis B virus (HBV)-mediated transformation and tumorigenesis have remained largely unclear, due to the absence of a relevant primary model system. Here we propose the use of human liver organoids as a platform for modeling HBV infection and related tumorigenesis. We first describe a primary ex vivo HBV-infection model derived from healthy donor liver organoids after challenge with recombinant virus or HBV-infected patient serum. HBV infected organoids produced cccDNA, expressed intracellular HBV RNA and proteins, and produced infectious HBV. This ex vivo HBV infected primary differentiated hepatocyte organoid platform was amenable to drug screening for both anti-HBV activity as well as for drug-induced toxicity. We also studied HBV replication in transgenically modified organoids; liver organoids exogenously overexpressing the HBV receptor NTCP by lentiviral transduction were not more susceptible to HBV, suggesting the necessity for additional host factors for efficient infection. We also generated transgenic organoids harboring integrated HBV, representing a long-term culture system also suitable for viral production and the study of HBV transcription. Finally, we generated HBV-infected patient-derived liver organoids from non-tumor cirrhotic tissue of explants from liver transplant patients. Interestingly, transcriptomic analysis of patient-derived liver organoids indicated the presence of an aberrant early cancer gene signature, which clustered with the HCC cohort on the TCGA LIHC dataset and away from healthy liver tissue, and may provide invaluable novel biomarkers for disease surveillance and development of HCC in HBV infected patients.

BACKGROUND

Persistent HBV infection is the leading cause of chronic liver cirrhosis and hepatocellular carcinoma (HCC) world-wide (MacLachlan, 2015; Di Bisceglie, 2009; An, 2018). A combination of viral and host factors determines whether an individual infected with HBV will be able to clear the infection or will become a chronic carrier. Characterized by its high host-species and organ-specificity, HBV infection and replication is thought to orchestrate an interplay between the immune system and viral-specific factors that eventually lead to the onset of HCC. Insights into the molecular mechanisms underlying HBV-induced HCC have largely been provided by epidemiological studies (El-Serag, 2012; Fattovich, Bortolotti, & Donato, 2008; Jiang et al., 2012; Sagnelli, Macera, Russo, Coppola, & Sagnelli, 2019), genome wide analysis of viral and host characteristics (Cancer Genome Atlas Research Network. Electronic address & Cancer Genome Atlas Research, 2017; Fujimoto et al., 2012; Huang et al., 2012; Ji et al., 2014; Sartorius et al., 2019; Shibata & Aburatani, 2014; Sung et al., 2012)), as well as by studies performed in in vitro settings using hepatoma cell lines (Thomas & Liang, 2016; Zhang, Wang, & Ye, 2014).

However, a major deficiency attributed to the strict viral host and cell type tropism is the limited availability of relevant animal or in vitro model systems to study HBV infection. Chimpanzees remain the only animal model that supports the full HBV replication cycle, while available hepatoma cell line models are unsuitable for delineating the molecular steps towards tumorigenesis as they differ substantially from primary cells in their already tumor-derived gene expression profiles (Protzer, 2017). These systems have inherent limitations resulting in poor predictive value for clinical outcome (Allweiss & Dandri, 2016). Primary hepatocytes present the gold standard model system for HBV research in vitro, especially with recent studies that have demonstrated a significant increase in the half-life of these cultures (Xiang et al., 2019). However they are difficult to obtain and, since they cannot be expanded, are not usually available in quantities sufficient to perform large-scale analyses (Hu, 2019). Induced pluripotent stem cell (iPSC)-derived hepatocytes which are susceptible to HBV infection and support replication are also a useful model for studying host-virus determinants of replication (Kaneko et al., 2016; Nie et al., 2018; Sakurai et al., 2017; Xia et al., 2017). However, iPSC-derived hepatocyte models cannot be patient derived, limiting studies to only ex-vivo infection systems and limiting the possibility of patient-specific personalized treatment approaches (Torresi, 2019; Nantasanti, 2016). As a consequence of deficiencies in available model systems, despite its fascinating biology, many questions regarding the life cycle of HBV and its mechanisms of persistence,

including HBV-induced molecular events underlying tumorigenesis, remain largely unexplored in primary settings, and key viral and host players involved remain unknown.

The dependence of hepatocytes on spacial and matrix-derived signals had until recently prevented their long-term in vitro culturing. The organoid culture technology involves the generation of cell-derived genetically-stable in vitro 3D-organ models of human origin. We have previously established a primary liver culture system based on isolation and expansion of primary cells that allows for the long-term expansion of liver cells as organoids (Huch et al., 2013; Huch et al., 2015). In this culture system, isolated adult hepatic cells are expanded through multiple passages in an optimized medium (EM) without induction of genomic alterations (Huch et al., 2015). When switched to differentiation medium (DM) where proliferation signals are removed and ductal (progenitor) fate is inhibited, liver organoid cultures differentiate into functional hepatocytes in vitro as exemplified by their polygonal cell shape (Figure 1a), and hepatocyte functions including Albumin production and Cytochrome C3A4 expression and activity (Huch et al., 2015). Here we use the human liver organoid platform to model and study HBV infection and replication, as well as related tumorigenesis in patient-derived organoids generated from HBV-infected donors. This expandable model yields patient-specific organoids in quantities amenable to molecular and functional characterization, and allowed us to generate a living biobank of HBV infected patient-derived cells amenable to downstream genomic, transcriptomic and proteomic analysis as well as screening for HBV-directed therapeutics. We first describe the ex-vivo HBV-infection of healthy donor (hD)-derived liver organoids, as a model to investigate the viral infection and replication in hepatocytes. We use the HBV infected organoid model as a platform for drug screening that can measure both drug-induced anti-HBV transcription and replication activity as well as drug-induced toxicity. We also demonstrate that transgenic modification of liver organoids provides an in vitro mechanistic platform to study the molecular determinants of HBV infection and replication. Finally, we conduct transcriptomic analysis of HBV-infected patient-derived organoids and describe the discovery of an early cancer gene signature, a potentially invaluable prognostic biomarker for HCC.

Results

Human liver organoids allow modelling of HBV infection in vitro

We first used the previously characterized liver organoid platform (Huch et al., 2015) generated from healthy donors to set up a novel ex-vivo HBV-infection system to study HBV replication. Liver organoids from healthy donors were grown in either expansion media (EM) or differentiation media (DM) (Figure 1a) for 7 days prior to infection with recombinant HBV generated from HepG2.2.15, a HepG2 cell line subclone stably expressing HBV (Figure 1b-c). As control for the inoculum, we also infected organoids with heat inactivated HBV (HI). HBV infection and replication were validated by quantifying the levels of HBV DNA in the supernatant (Figure 1c), intracellular HBV RNA (Figure 1d), HBV-specific proteins by immunofluorescence microscopy (Figure 1e) and intracellular covalently closed circular DNA (cccDNA) from infected organoids (Figure 1f). HBV DNA was detected in organoid culture supernatants from four days post infection, but not from the heat-inactivated virus infected cells, indicating successful HBV replication (Figure 1c). Differentiated organoids maintained in DM were more efficiently infected and produced higher viral titers than organoids maintained in EM (Figure 1c-d). The RNA intermediates necessary for protein production and viral replication (HBV pol and Hbx) were present in infected DM organoids and detected by RT-PCR analysis, but not in the heat-inactivated virus infected cells (Figure 1d). Immunostaining, using antibodies recognizing HBV core (HBcAg) showed specific nuclear and cytoplasmic staining in multiple infected healthy donor liver organoid lines, confirming the presence of foci of HBV replication in HBV-infected cells predominantly in infected DM organoids (Figure 1e and Figure 1-Figure Supplement 1). Furthermore, infection of DM organoids resulted in the production of cccDNA, a definitive marker of HBV replication, as detected by a qPCR-based cccDNA detection method of intracellular HBV DNA after digestion with a nuclease to specifically remove non-cccDNA (Figure 1f). Inoculum that lacks cccDNA was used as a negative control for the cccDNA-specific qPCR and HBV plasmid DNA was used as a positive control (Figure 1f). HBV replication, infection and spread appeared to be persistent until 8 days after infection when viral production dropped significantly, likely because of the limited half-life of differentiated organoids in culture (Figure 1-Figure Supplement 2). Periodic culturing of the organoids in EM in order to stimulate the recovery and proliferation of the organoids modestly extended the half-life of the infected cultures, where viral production was maintained for approximately one month post infection (Figure 1-figure supplement 2). To determine whether the organoids are capable of producing infectious HBV, supernatants containing virus

produced by organoids, were collected, concentrated and used for subsequent spinoculation of healthy donor (hD) organoids. As shown in Figure 1g, infection of hD organoids with organoid-produced HBV resulted in expression of intracellular HBV RNA, indicating that organoids produce infectious viral particles. Growth of viral isolates from patient material has been limited by the lack of an adequate primary model system. However, differentiated organoids were able to support infection and replication when challenged with HBV infected patient sera, as shown by production of viral DNA, expression of viral transcripts and positive immunostaining for HBsAg (Figure 1h and (Figure 1-figure supplement 3). Differentiated liver organoids therefore provide a useful ex vivo HBV infection platform in which the role of specific host and viral factors can be investigate.

Ex vivo HBV-infected liver organoids are a viable platform for anti-viral drug screening and drug induced toxicity

We next examined whether the ex vivo infected liver organoid platform would be amenable to anti-HBV drug screening to monitor antiviral activity and drug-induced toxicity of two different drugs, Tenofovir and Fialuridine, according to the schematic in Figure 2a. Tenofovir is a nucleoside reverse transcriptase inhibitor which inhibits the reverse transcription of HBV pre-genomic RNA to DNA. Fialuridine, also a nucleoside analogue that inhibits reverse transcription, was shown to cause severe hepatotoxicity in patients (McKenzie et al., 1995). In the organoids, HBV viral DNA production in the culture supernatant was inhibited by both Tenofovir and Fialuridine in three independent healthy donor (hD) derived organoids; whereas, as expected, RNA levels remained the same (Figure 2b). Therefore, the organoid ex vivo-infection platform not only allows measurement of drug-induced antiviral activity, but also offers insight into the mechanism of drug action by allowing delineation of which step of the HBV life cycle is targeted and inhibited. As expected, treatment of HepG2.2.15 cells with Tenofovir and Fialuridine resulted in similar decreases in released HBV DNA, but no change in intracellular HBV RNA levels (Figure 2c), reaffirming the mechanism of action of these drugs in a cell-line model of HBV replication. Due to the well-established detrimental effects of Fialuridine on viability of primary human hepatocytes, we sought to evaluate Fialuridine-induced toxicity on primary human liver organoids as well as in HepG2 cells. We measured the viability of organoids and HepG2 cells using the alamarBlue viability assay and by monitoring their phenotype upon Fialuridine and Tenofovir treatment using microscopy. HepG2 cells demonstrated no change in cell viability upon treatment with Tenofovir and increasing concentrations of Fialuridine as compared to the mock treated

cells (Figure 2d). The phenotype of HepG2 cells was also comparable across all treatments as observed by microscopy (Figure 2e). Strikingly, the liver organoids treated with Fialuridine at as low a concentration of 1µM demonstrated a significant reduction in viability as measured by AlamarBlue assay when compared to mock treated cells (Figure 2f and Figure 2-figure supplement 1a). The organoids treated with higher Fialuridine concentrations (5-20µM) as well as with 20µM Tenofovir also demonstrated impaired viability (Figure 2f and Figure 2-figure supplement 1a). The decreased cell viability was also apparent in the phenotype of the 1-20µM Fialuridine-treated and 20µM Tenofovir-treated organoids compared to vehicle control as observed by microscopy (Figure 2g and Figure 2-figure supplement 1b). This highlights that Fialuridine-induced toxicity is evident and quantifiable in the primary human liver organoid model but not in the HepG2.2.15 model of HBV replication. Thus, we demonstrate that ex vivo infected differentiated liver organoids support the full replication cycle of HBV and serve as an ideal novel primary platform for drug screening and to elucidate the molecular events underlying HBV replication. Moreover, human liver organoids serve as an ideal platform for monitoring drug induced toxicity in pre-clinical studies.

HBV replication can be investigated in transgenically-modified liver organoids

We previously observed higher HBV infection efficiency in DM organoids as compared to EM organoids (Figure 1c). This correlated with higher levels of Sodium taurocholate co-transporting polypeptide (NTCP) expression, a cellular receptor expressed on the surface of hepatocytes implicated in HBV entry (Yan et al., 2012), in differentiated organoids as compared to organoids in EM (Figure 3a-b). Exogenous expression of NTCP in hepatoma cell lines was shown to confer susceptibility to infection (Yan et al., 2012) in line with our observed increased HBV infection in differentiated organoids, likely because of the higher level of NTCP expression. Since differentiated organoid cultures have a limited half-life, we sought to generate transgenically modified healthy donor (hD) organoids exogenously expressing NTCP under expansion conditions (Figure 3c-e and Figure 3-figure supplement 1a-b) in order to improve infection efficiency and facilitate downstream analyses and investigation of the molecular events involved in HBV replication. We used a lentiviral construct harboring the coding sequence of Flag-tagged NTCP ubiquitously expressed under a CMV promoter, followed by a blasticidin selection marker (Figure 3c). Immunofluorescence experiments performed on NTCP-liver organoids in expansion phase confirmed high levels of NTCP protein expression correctly localized to the cellular membrane (Figure 3e and Figure 3-figure supplement 1b). Cholesterol target

genes were induced in response to statin treatment in NTCP transgenic organoids, confirming the functionality of exogenously expressed NTCP (Figure 3-figure supplement 1c). We then evaluated viral production following HBV infection in transgenically modified-NTCP organoid lines as compared to parental lines (Figure 3f-g). Interestingly, comparable levels of HBV DNA and HBS antigen levels were observed in the supernatants of both parental and NTCP expressing organoid lines (Figure 3f-g), suggesting that expression of NTCP alone is not sufficient to improve HBV infection rate in liver organoids grown in EM (Figure 3f-g and Figure 3-figure supplement 1d).

To further highlight the ability of liver organoids to be transgenically modified, we produced a long-term, expandable, primary HBV producing liver organoid model system that can be used to study HBV transcription events. We utilised a lentiviral construct to produce transgenic organoid lines containing an integrated copy of HBV (Figure 3-figure supplement 2). Interestingly, when the HBV genome was placed downstream of the CMV promoter (Figure 3-figure supplement 2c), transgenic organoids, while efficiently expressing HBV RNA, did not support replication, as demonstrated by the low levels of HBV DNA in the culture supernatant (Figure 3-figure supplement 2d), pointing to CMV promoter-induced transcriptional interference with promoter usage required for mRNA transcription of individual HBV genes. Removal of the CMV promoter to generate “lenti-HBV” (Figure 3-figure supplement 2e-f) allowed for the generation of replication-competent, expandable, long term, hD transgenic lenti-HBV organoid lines, in which transcription from the HBV transgene results in protein and viral production (Figure 3h-i, Figure 3-figure supplement 2f). Although lacking cccDNA, this model system provides a primary platform to screen for inhibitors of HBV transcription and is a primary-cell alternative to the HepG2.2.15 cell lines which also do not produce cccDNA, for studies into HBV pathogenesis. Thus, the amenability of human liver organoids to transgenic modification enables investigation of HBV replication and in depth characterization of the molecular events involved.

HBV-infected patient-derived liver organoids contain functional hepatocytes

The ability to generate a patient-derived primary model is a key advantage of using the liver organoid platform. We applied the previously characterized method to generate liver organoids from healthy donors (Huch et al., 2015) to generate novel patent-derived organoids from HBV-infected individuals undergoing liver transplantation (Figure 4a). The explant used for generating patient-derived organoids was HBV-infected, chronically cirrhotic liver tissue obtained from eleven explanted livers from people

infected with HBV (Figure 4a and b, Table 1). We generated and expanded organoid cultures from fresh and frozen explant tissue from all donors with similar efficiency (data not shown).

Non-tumor, HBV-infected, patient-derived (infected patient (iP)) organoids were expanded in culture (EM) and displayed proliferation rates (Figure 4b and data not shown) and expression of progenitor markers LGR5, KRT7, HNF4α, and Sox9 (Figure 4c) comparable to that of healthy donor (hD) organoids. When grown in differentiation medium (DM), in which proliferation signals are removed and the progenitor fate is inhibited, liver organoid cultures from both healthy and HBV-infected sources acquired hepatocyte fate and differentiated into functional hepatocytes, similar to previously obtained data for healthy liver organoids (Huch et al., 2015). In DM, both hD and iP liver organoid cultures (Huch et al., 2015) showed increased expression of hepatocyte-specific genes Albumin and Cytochrome C3A4 , and the cellular receptor implicated in HBV hepatocyte entry NTCP, concomitant with decreased expression of the stem cell-specific gene LGR5 (Figure 4d and Supplementary Figure 6). None of the iP organoids showed signs of HBV production at the RNA, DNA or protein level (data not shown), suggesting that adult stem cells from which the liver organoids are generated are not infected by detectable levels of HBV. At the phenotypic level, while EM organoids grew larger in size and were translucent, differentiated iP organoids showed hepatocyte morphology and a thickening of the outer cell layer, comparable to hD organoids (Figure 4e and Figure 4-figure supplement 1a) and produced comparable levels of albumin as detected by immunofluorescence staining (Figure 4e and Figure 4-figure supplement 1b). Thus, non-tumor HBV iP and hD organoids display comparable phenotypes, retain the capacity for differentiation and are conducive to downstream genomic, transcriptomic and proteomic analysis.

HBV infected patient-derived liver organoids display a distinct early gene expression signature

The early detection of HBV-related HCC is a challenge that remains critical to direct optimal clinical management of the disease. Despite widely practiced periodic surveillance of patients with cirrhosis, patients with HCC are mostly diagnosed in a late stage. The presence of diagnostic biomarkers for early events in liver cell tumorigenesis would therefore be invaluable to early detection. In order to identify potential early biomarker genes for HBV-induced HCC, we performed mRNA sequencing of the organoid lines derived from HBV-infected patient (iP) and compared their gene expression profile to that of organoids derived from healthy donors (hD). We performed hierarchical clustering of protein-coding differentially expressed genes obtained from the comparison between organoids of five hD

organoid lines with five iPs (Figure 4f, Table 1). The iP organoid lines were seeded from five HBV mono-infected patients with cirrhotic liver, four of whom presented with small tumors at the time of explant (Figure 4f, Table 1). Interestingly, although the hD and iP organoids were phenotypically indistinguishable, the iP organoids clustered separately from the healthy donors (Figure 4f). This comparison resulted in identification of an iP-characteristic "gene signature" (Figure 4f and Table 2). We then ranked the differentially expressed genes according to the relative distance of their expression in hD versus iP derived organoids and identified a group of 33 putative early biomarker genes (Figure 4g). GO-term and KEGG-pathway analysis revealed that the "early signature" genes were enriched in metabolic pathway-associated genes (Table 3). Among these, CCNA1, STMN2, which we found were upregulated in the non-tumor patient-derived organoids, were previously identified to be upregulated in HCC (Allain, Angenard, Clement, & Coulouarn, 2016; Chen et al., 2019; Gao et al., 2008; Paradis et al., 2003). Conversely, WNK2, RUSC2, CYP3A4 and RGN, among the significantly downregulated genes in the non-tumor iP organoids have been described as tumor suppressors downregulated in HCC (Allain et al., 2016; Ashida et al., 2017; Tao et al., 2011; Yamaguchi, 2015). Therefore, transcriptomic analyses of healthy vs. patient-derived organoids resulted in the identification of an HBV infection early gene signature and possible biomarkers for HBV infection.

Transcriptomic analysis of HBV-patient derived organoids result in identification of cancer gene signature

We then applied this "early gene signature" derived from our analysis (Figure 4f) to all our liver organoid samples. Our subsequent analysis included 5 healthy donors (hD1-5), 10 HBV-infected samples (iP) and one donor that had previously been infected with HBV, but had subsequently cleared infection and displayed no aberrant phenotype (infected donor iD). Amongst the iPs, there were samples from patients that had HCC at the time of collection (iP-HBV-HCC); acute liver failure (iP-ALF-HBV); an HBV-infected cirrhotic liver without HCC, no acute liver failure or any coinfections (iP-BC); and HBV-HDV coinfected samples that had either HCC (iP-HCC-HBV+HDV) or acute liver failure (iP-ALF-HBV+HDV). Table 1 describes all patients, groups and clinical characteristics. The early signature when applied to all iP and hD samples, perfectly groups the healthy (grey) against the HBV-infected samples (black) (Figure 5a). HBV-infected iP organoids (purple) and the HBV/HDV co-infected iP organoids closely together (light blue). The signature also separates and groups together the non-infected samples (green), iP organoids derived from patients who had HCC (red) as well as those

derived from patients with acute liver failure (dark blue). Interestingly, the organoids generated from the infected donor (iD) who had cleared HBV infection (light orange), as well as the infected patient with cirrhotic HBV-infection (dark orange) clustered together and closely to the larger group of iP organoids derived from patients with HCC (red) (Figure 5a). This observation from iD clustering closely with iP-HBV-HCC indicated the presence of the early HCC-like gene signature in this infected donor liver despite clearance of HBV infection and absence of phenotypic and functional abnormalities at time of donation, an observation that may be important to considered for transplantation purposes and surveillance. In agreement, multidimensional scaling analysis of all iP and hD samples indicated that all hD organoids are clearly separated from the rest and tightly grouped together, while the iP organoids form separate groups corresponding to HDV coinfection, HCC, acute liver failure or previous/cirrhotic HBV infection (Figure 5b). We have therefore identified a specific gene signature/group which discriminates the hD and iP organoids among more complex classifications (Figure 5a-b). We applied this gene signature to all samples stored in The Cancer Genome Atlas Liver Hepatocellular Carcinoma (TCGA-LIHC) database, a depository of sequences from HCC patients. The application of this gene signature when mapped onto the relevant TCGA gene expression data distinctly separated the HCC samples from non-HCC tissue (Figure 5c). This important observation indicates that transcriptomic analysis of our patient-derived liver organoid model identified a novel early liver cancer gene signature in non-tumor HBV-infected patient-derived liver organoids, despite the absence of phenotypic signs of aberrant growth. Thus, HBV-infected patient-derived liver organoids are a novel primary 3D cell culture model that resemble the diseased tissue of origin and can be used from genomic, transcriptomic, proteomic and clinical applications to identify biomarkers for disease states during HBV infection.

Discussion

Human liver organoids are a novel in vitro primary model system that support HBV infection and replication, can be utilized as a platform to study HBV pathogenesis as well as for anti-HBV-drug screening, can be transgenically modified for downstream mechanistic and functional assays, and can be seeded from HBV-infected patient liver for personalized molecular and functional analysis (Figure 5). Healthy donor liver organoids were efficiently infected with both recombinant virus as well as HBV infected patient serum, expressed HBS Ag and HBV core proteins, produced cccDNA and infectious HBV in the culture supernatant indicting that liver organoids support the full HBV replication cycle (Figure 1). Human liver organoids therefore serve as an invaluable tool in the field of HBV-research to investigate the molecular mechanism underlying HBV replication in a primary cell system that is expandable and biobankable.

We demonstrated that the ex vivo infected organoid replication platform is amenable to screening for potential inhibitors of HBV replication and can provide insights into both HBV-directed anti-viral activity as well as drug-induced toxicity. The ability to measure different readouts of HBV replication at the level of HBV mRNA gene expression, or viral production by quantitation of HBV DNA or S Antigen present in the culture supernatant of HBV-infected liver organoids, can provide insight into the distinct steps in the HBV life cycle that may be targeted upon drug treatment. This is highlighted by our studies using the HBV-directed drugs Tenofovir and Fialuridine (Figure 2a), which as expected did not affect the levels of intracellular HBV RNA, but blocked HBV replication by inhibiting the reverse transcription step which converts HBV pre-genomic RNA to DNA, as we observed by decreased HBV DNA levels. A critical aspect of potentially therapeutic novel drugs which causes failure within the drug development pipeline is toxicity. While Fialuridine treatment of HBV infected human liver organoids efficiently inhibited HBV replication, it also caused significant toxicity in the liver organoids. The importance of this pre-clinical human liver organoid model to measure drug-induced toxicity is highlighted by the results of a phase II clinical trial conducted in 1993 to evaluate Fialuridine as a novel HBV-anti-viral drug (Eli Lilly Trial H3X-MC-PPPC, NIH protocol #93-DK-0031). Although the preliminary results of the trial were promising with reduced levels of HBV DNA in patients, the study was terminated on an emergency basis by week 13 because of serious hepatotoxicity in seven patients of which 5 died and two required emergency liver transplantation (McKenzie, 1995). This compound successfully passed pre-clinical toxicity studies, but the expression of a nucleoside transporter in human mitochondria may be responsible for the human-specific mitochondrial toxicity

caused by Fialuridine (Lee, Lai, Zhang, & Unadkat, 2006). In the primary human liver organoid system, the toxicity of Fialuridine is significant and quantifiable (Figure 2e-f) but was not observed in the human HepG2 hepatoma cell line indicating that human liver organoids can more accurately predict clinical outcomes of drug treatment. Thus the HBV infected organoid platform can be used as an important pre-clinical, primary hepatocyte screening platform for both discovery of candidate new drugs targeting HBV transcription and replication, as well as their potential toxicity.

When cultured under differentiating growth conditions, the expression of the HBV receptor NTCP increased significantly in liver organoids. Consistent with the observed higher NTCP levels, in vitro infection of differentiated organoids with HBV led to higher levels of infection and replication. To obtain an expanding long term HBV infected replicating cultures of human liver organoids, using transgenic modification by lentiviral transduction, we generated liver organoids that exogenously expressed membrane-localized NTCP under expansion conditions. Surprisingly, the presence of NTCP did not result in more efficient infection of organoids, suggesting that although necessary, NTCP alone may not be sufficient for optimal infection (Figure 3). Consistent with our observations, HepG2 cell lines exogenously expressing NTCP, while susceptible to infection are inefficiently infected with HBV and require high viral titers (Iwamoto et al., 2014; Yan et al., 2012). These observations are suggestive of the potential necessity for additional (co)receptors or downstream factors necessary for optimal infection in hepatocytes. Using lentiviral transduction, we also generated polyclonal liver organoids that contain integrated full length HBV genome, which efficiently produced HBV under expansion conditions. This model, similar to HepG2.2.15 cell, although not a cccDNA generating model of productive HBV infection, is a useful primary human liver model to investigate HBV transcription and HBV-directed drugs.

Recently alternative liver organoid model systems derived from human (induced) pluripotent stem cells (Kaneko et al., 2016; Nie et al., 2018; Sakurai et al., 2017; Xia et al., 2017) as well as primary human hepatocyte coculture systems (March et al., 2015; Xiang et al., 2019)(Xiang et al., 2019) have been developed that can be used to study hepatitis B virus infection. However, the human liver organoid platform offers two main advantages over these model systems. The first and most important is that HBV infected patient-derived organoids resemble the diseased tissue of origin, as demonstrated by our gene expression studies (Figure 5). Second, the organoid platform allows the possibility of expansion and biobanking, ensuring the availability of sufficient samples for downstream analyses. Therefore, while primary human hepatocytes and iPSC models, similar to the ex vivo infection of hD human liver

organoids we describe here, provide reliable ex vivo infection models for studies on HBV, the human liver organoid platform is uniquely suitable for long term, patient-derived studies.

Early surveillance of the changes in gene expression or biomarkers that predict the occurrence of HCC is critical to enable patients to receive timely and successful treatment. Paving the way for personalized therapy of HBV infected patients, liver organoids can be seeded from infected patient liver resection, at different stages of the disease. Comparison of the gene expression profiles of healthy donor to HBV-infected patient-derived liver organoids, and further HDV co-infected and acute liver failure patient sub-groups point to the extent to which organoids reflect the biology and represent the transcriptomic profiles of the primary non tumor tissue of origin. Interestingly, consistent with the absence of infection of liver stem cells from which organoid cultures are seeded, we found no sign of viral production in the non-tumor HBV infected patient-derived liver organoid lines. Thus, the observed HBV infected patient-specific gene expression profile is likely generated from chronic uninfected bystander cells. Our observations are consistent with the notion that the gene expression profile of the tumor microenviroment may serve as an important biomarker of HCC as bystander cells are chronically exposed to released HBV proteins despite their uninfected status. Indeed, our data indicates that HBV infected non tumor patient-derived liver organoids exhibit an early cancer gene profile, as shown by comparison to the TCGA-LIHC database. The identification of early aberrant gene regulatory networks and biomarkers that drive HBV-mediated HCC, detectable at an early non-tumor stage without phenotypic signs of tumorigenesis, allows for patient-specific surveillance of disease progression and provides a screening platform for candidate drugs that guide personalized treatment by targeting early stages in HBV-mediated HCC.

Figure 1

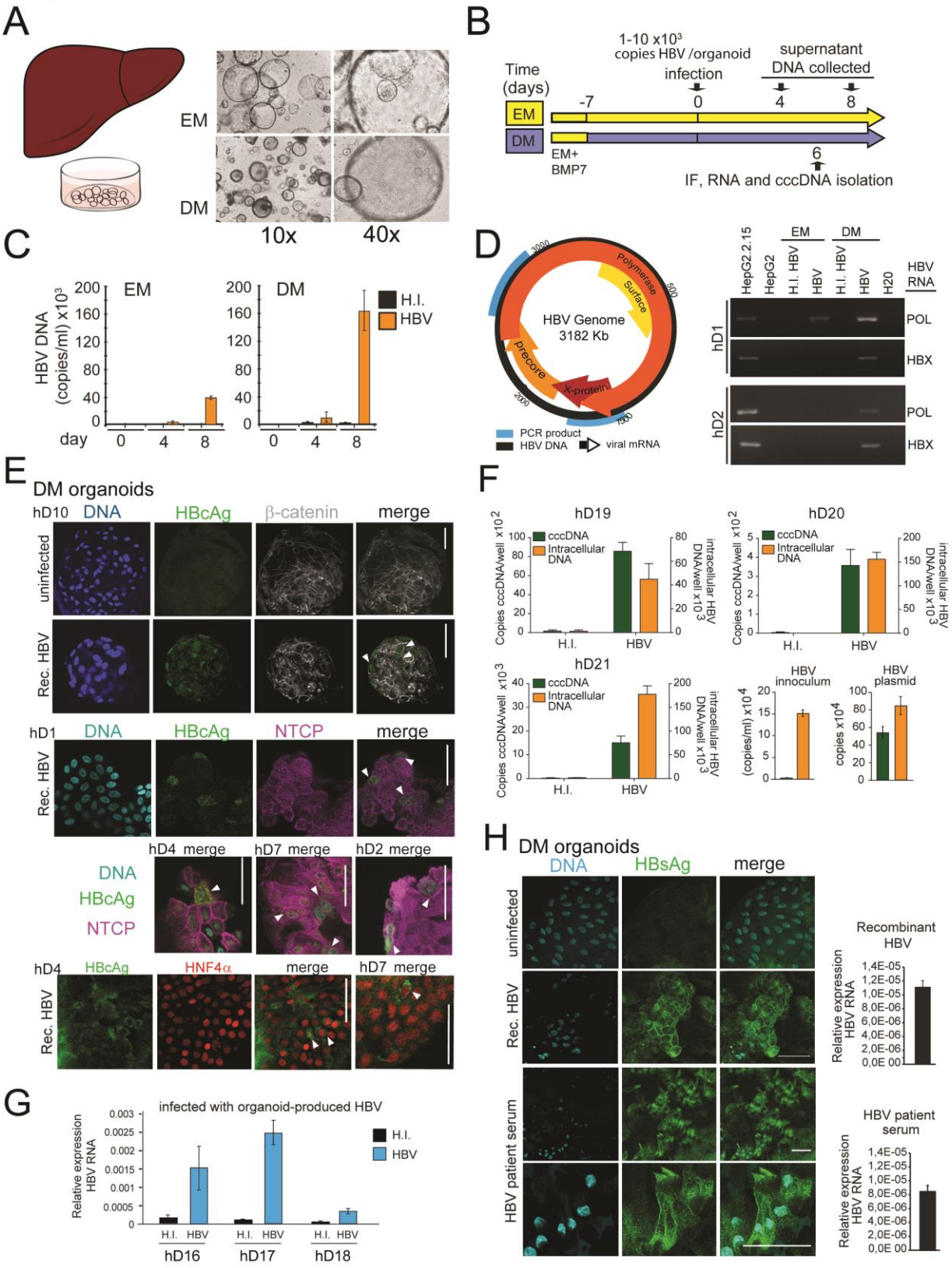

Fig. 1: Modeling HBV infection in vitro using human liver organoids (A) Representative images of liver organoids in EM and DM (B) Experimental design of infection experiments. Arrows indicate the time points for HBV detection. (C) Levels of HBV DNA in supernatant of infected organoid cultures were quantified at indicated times by real time PCR and compared to the cultures challenged with HI virus. (D) Schematic of the HBV genome showing ORFs (arrows) and the localization of PCR products (blue boxes). The agarose gel demonstrates expression of HBX and POL genes by nested PCR performed on cDNA obtained from two in vitro infected healthy donor (hD) organoid lines. (E) Immunofluorescent staining showing the expression of HBcAg (green) together with NTCP (magenta), β-catenin (grey) or HNF4α (red) performed in different hD organoids 6 days after HBV infection in differentiation medium. (F) Quantification of total HBV DNA (orange) and cccDNA (green) from intracellular DNA purified from three healthy donors (hD) organoid lines 6 days post infection with HBV under DM condition. Quantification of total HBV DNA and cccDNA is also shown from supernatant of infected organoids (inoculum) and from double stranded HBV plasmid (as positive control for cccDNA) (G) Expression of intracellular HBV RNA relative to beta 2 microglobulin in three hD organoid lines infected with organoid-produced HBV (concentrated from pooled supernatants of organoid cultures infected with HepG2.2.15-produced HBV). (H) Immunofluorescent staining showing the expression of HBsAg (green) in DM organoids infected with recombinant HBV and patient serum. Scale bars represent 50 µm. Bar graphs show total HBV RNA levels in the culture at the time of staining.

Figure 2

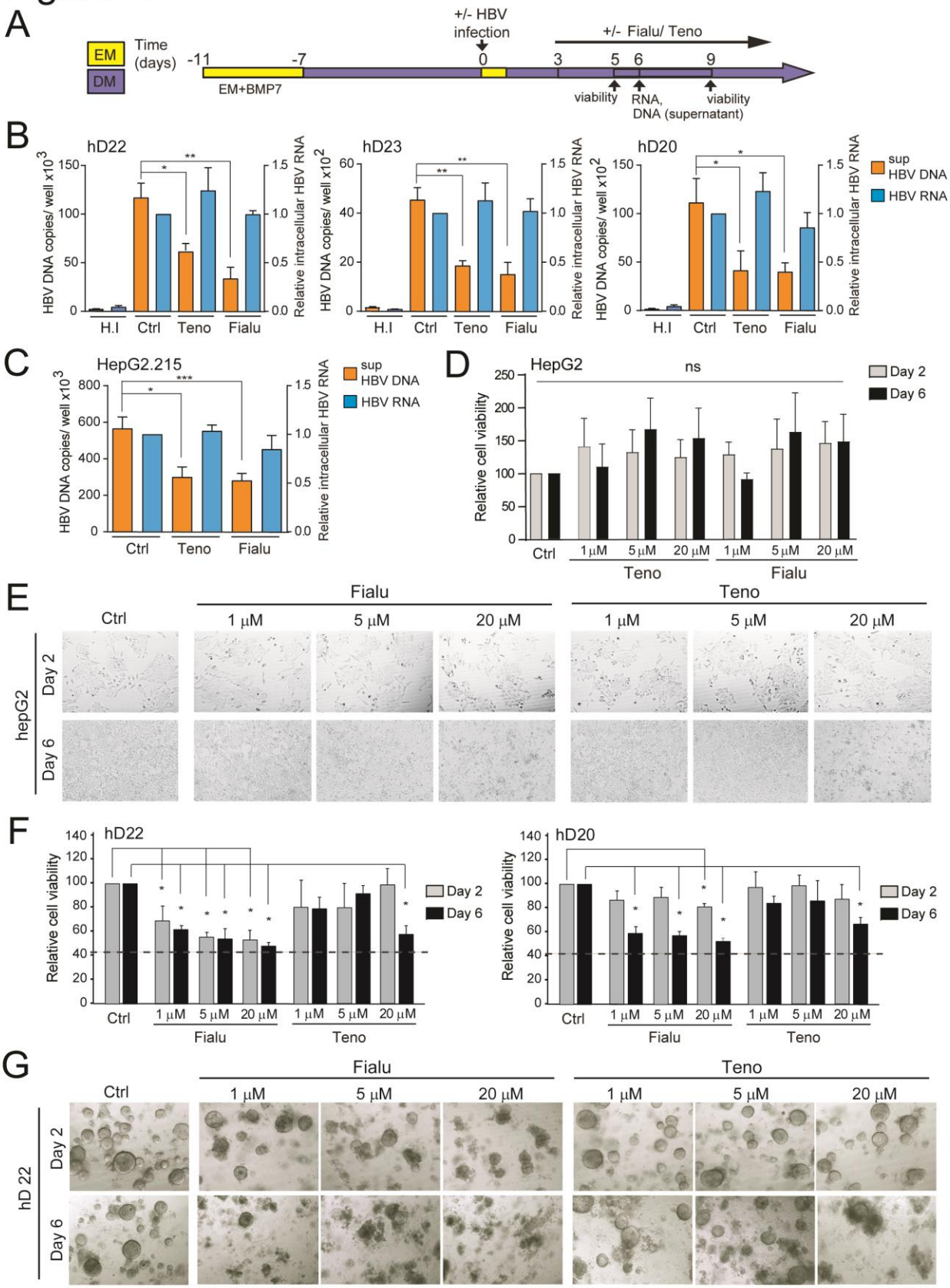

Fig. 2: HBV infected liver organoids as a model for HBV antiviral drug screening and toxicity (A) Experimental design of drug treatment of HBV infected liver organoids followed by assessment of antiviral activity and toxicity. Arrows indicate time points for HBV detection or assessment of viability. Levels of HBV DNA in the supernatant and intracellular HBV RNA were quantified by real time PCR and RT-PCR respectively for three independent healthy donors (B) and HepG2.2.15 cells (C) upon treatment with control vehicle, Fialuridine (10μM) or Tenofovir (10μM) as indicated. Data are shown as mean ± SD of at least 3 replicate treatments $*P < 0.05$; $**P < 0.01$. (D) Relative viability of HepG2 cells was measured using the AlamarBlue cell viability assay after treatment with vehicle control, Fialuridine or Tenofovir for 2 or 6 days as indicated, normalized to vehicle control and plotted as the average of percent viability ± SD (n=3) (n.s = not significant) (E) Representative bright field images taken of HepG2 cells treated with antiviral drugs for 2 or 6 days as indicated. (F) Bar diagrams representing relative cellular viability of hD liver organoids after 2 or 6 days of treatment with Fialuridine or Tenofovir at the different concentrations indicated using the AlamarBlue cell viability assay. All values are normalized to the vehicle treated control and plotted as the average of percent viability ± SD (n=3). The dotted line represents the lower limit of quantification based on values obtained from wells free of organoids containing the BME matrix only. (G) Representative bright field images taken of liver organoids treated for 2 or 6 days with the vehicle control or increasing concentrations of the antiviral drugs Tenofovir or Fialuridine as indicated.

Figure 3

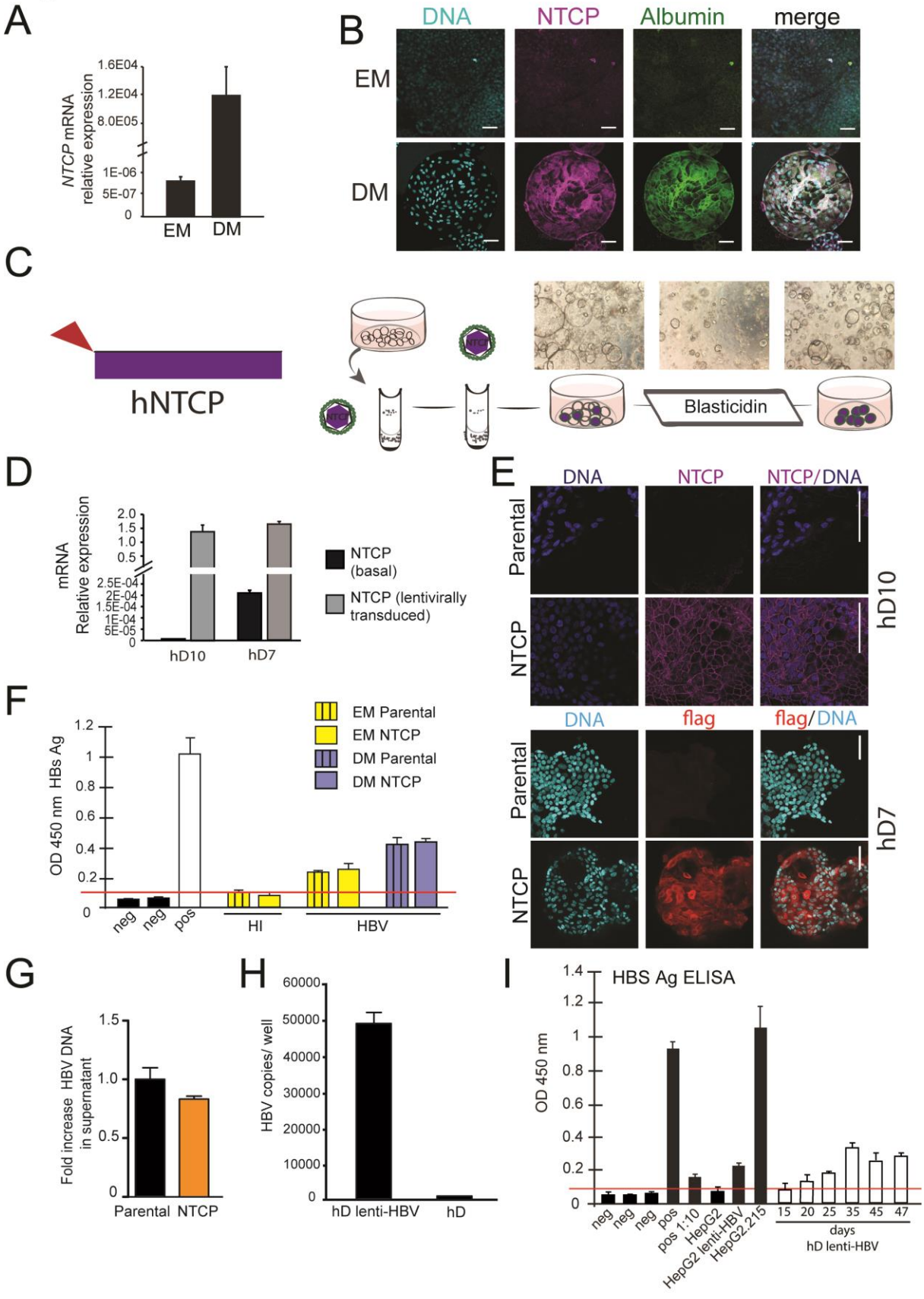

Fig. 3: Lentivirally transduced transgenic liver organoids in the study of HBV (A) mRNA expression levels of the HBV receptor NTCP in undifferentiated (EM) and differentiated (DM) organoids (n=3); mRNA levels were calculated according to the 2ΔCt method using GAPDH as reference gene. (B) Immunofluorescent staining showing the expression of NTCP (magenta) in EM and DM organoids. Nuclei were counterstained with Hoechst 33343 (cyan). Scale bars represent 50 µm. (C) Schematic representation of the experimental procedure for the transduction experiments. Following infection with a lentiviral vector expressing Flag-NTCP, organoids were selected with blasticidin for 5 days in order to obtain lines expressing NTCP in the expansion phase. (D) Levels of expression of NTCP were evaluated by RT-PCR in the untransduced (Parental) and the transduced (NTCP) lines. Expression of NTCP was calculated according to the 2ΔCt method using the housekeeping gene GAPDH as reference gene and confirmed by immunofluorescence staining targeting NTCP (magenta) or Flag (red) (E). (F) HBsAg released in the supernatant of parental and NTCP organoid lines grown in EM or DM 10 days after HBV infection was detected by ELISA. Challenge with heat inactivated virus was used to control for HBsAg present in the inoculum. Pos and neg bars correspond to positive and negative controls provided by the kit manufacturer. Threshold for positivity (red line) was calculated as the average OD + 2SD of negative controls. (G) HBV DNA in the supernatant of NTCP expressing organoid cultures was quantified 5 days after infection and compared to DNA detected in the supernatant of untransduced HBV infected organoids (n=3). Bars represent fold increase in HBV DNA detected in the supernatant, untransduced HBV infected organoids were used as reference. Relative amounts of (H) HBV RNA and (I) HbS antigen produced by hD lenti-HBV organoid lines.

Figure 4

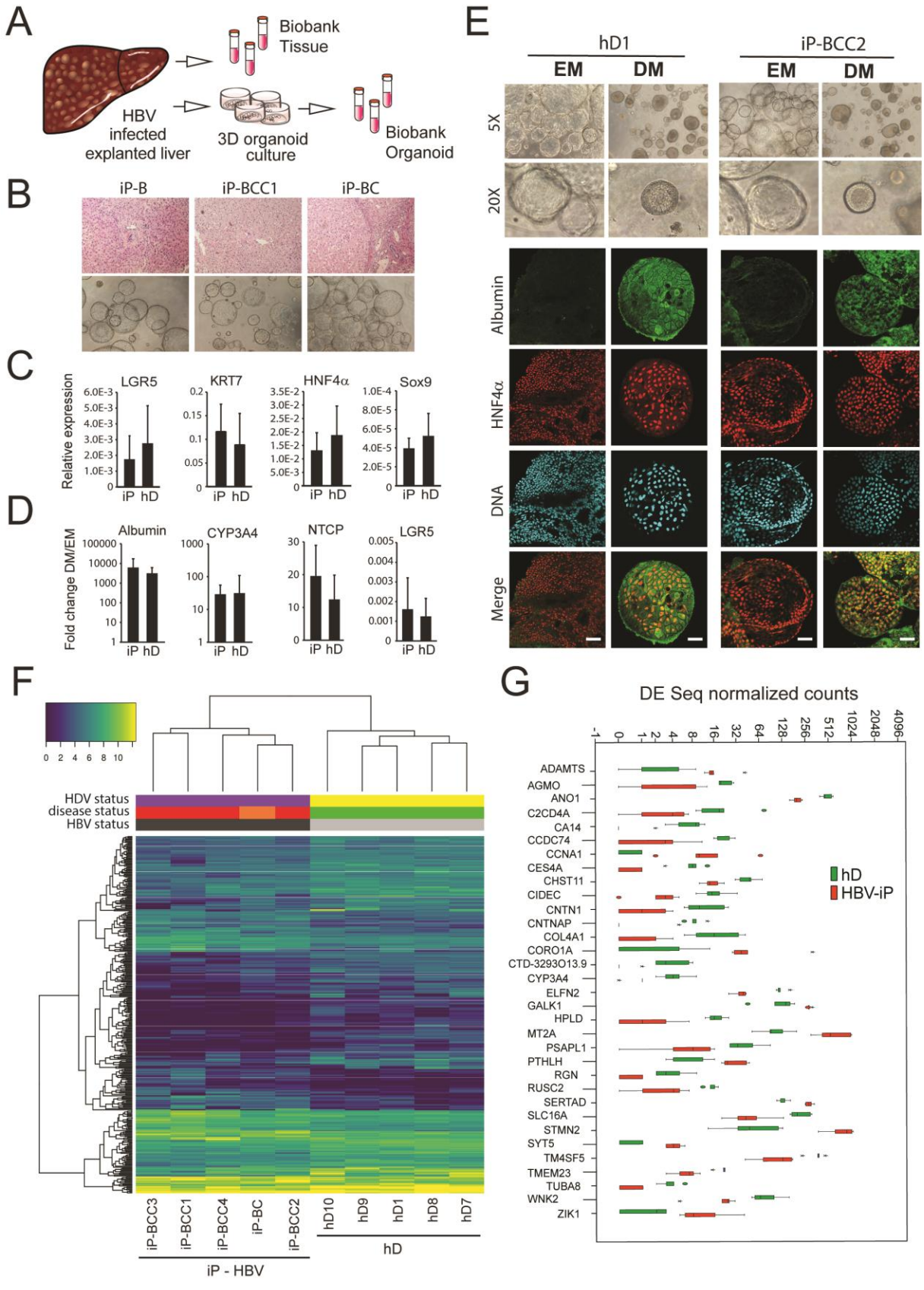

Fig. 4: Characterization of organoid cultures from liver explants of HBV-infected patients. (A) Representative panel showing the procedure to generate organoid cultures or biobanks from liver tissue. (B) Hematoxylin-eosin stained sections of explanted liver tissue and phase contrast pictures showing the morphology of liver organoids derived from HBV infected individuals. (C) Expression profile of the progenitor markers LGR5, KRT7, HNF4α, and Sox9 in EM (undifferentiated) organoids derived from liver of healthy donors (hD) (n=4) and HBV infected individuals (iP) (n=5). Levels of expression were calculated according to the 2ΔCT method using GAPDH as reference gene (D) Differentiation capacity of organoid cultures derived from liver of hDs (n=4) and iPs (n=5). Bars represents fold difference in the expression of hepatocyte-specific genes Albumin, Cytochrome CYP3A4, NTCP and of the progenitor-specific gene LGR5 in DM (differentiated) cultures compared to EM organoids using the 2ΔΔCT method. (E). Immunofluorescent staining targeting albumin (green) and HNF4α (red) was performed in EM and DM organoids. Phase contrast images, depicting the morphology of the cells are shown as reference. (F) Hierarchical clustering heatmap of differentially expressed genes derived from the comparison between the group of five hDs and five iPs presenting HBV infection and HCC (four out of five). (G) Box plot of DESeq normalized counts of 33 putative biomarker genes obtained from healthy donor organoids (depicted in green) or obtained from HBV-iP organoids (depicted in red).

Figure 5

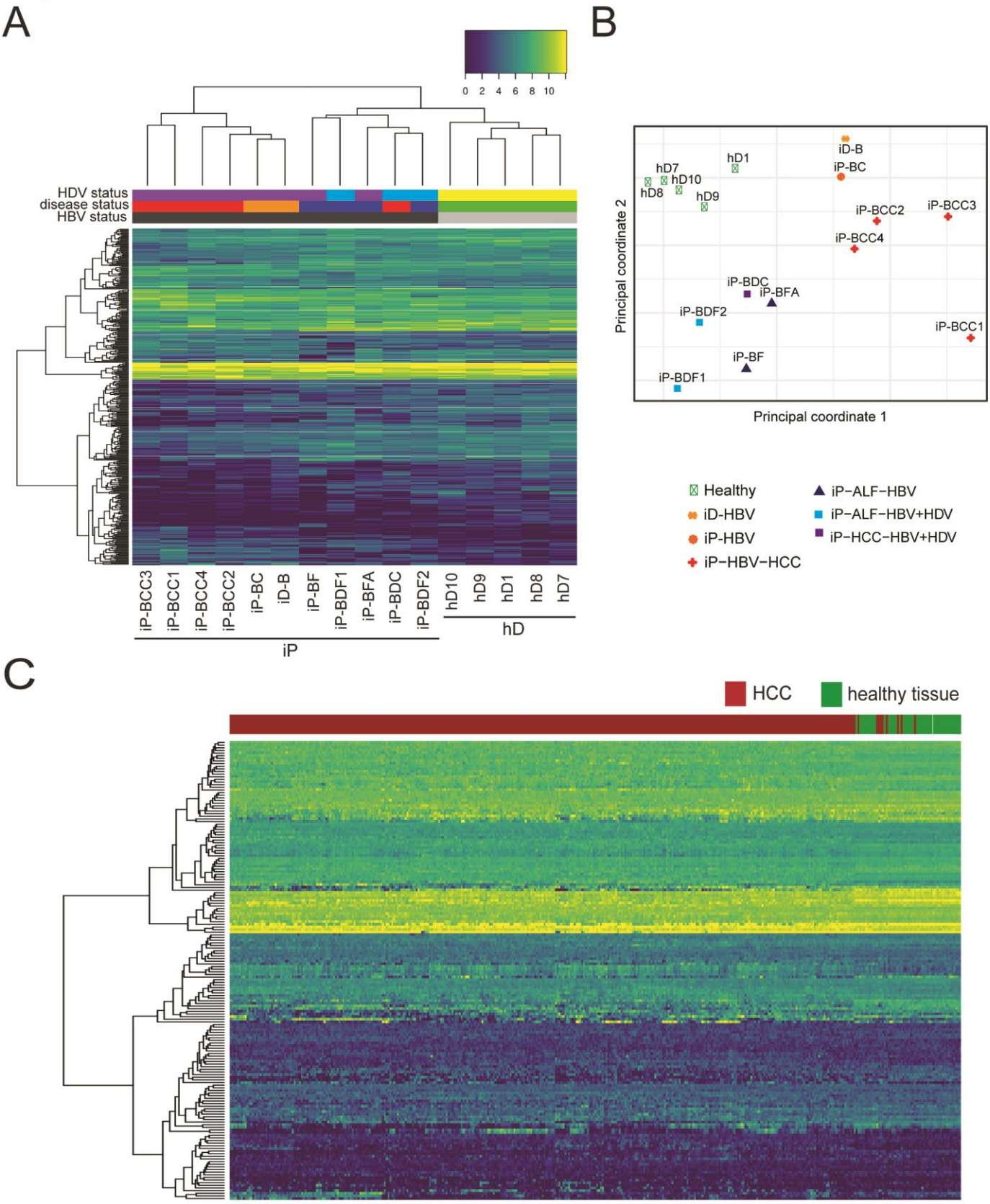

Fig. 5: Identification of early HCC gene signature in non-tumor iP-derived organoids. (A) Hierarchical clustering heatmap of all iP and hD samples depicting the grouping and expression levels of protein coding differentially expressed genes derived from the comparison between the group of five hDs and five iPs presenting HBV infection and HCC (four out of five). Coloured bars on top of the heatmap indicate HBV status (black for HBV positive patients, gray for healthy donors), disease status (red for HBV positive HCC, orange for HBV positive without HCC, blue for HBV positive acute liver failure, green for healthy donors), and HDV coinfection status (purple HBV positive HDV negative, light blue for HBV positive HDV positive, yellow for healthy donors). (B) Multidimensional scaling plot of all iP and hD samples. (C) Hierarchical clustering heatmap of liver HCC gene expression data from 342 HCC tissue samples and 47 samples from matched nearby tissue from TCGA using the HBV iP versus hD gene signature.

Figure 6

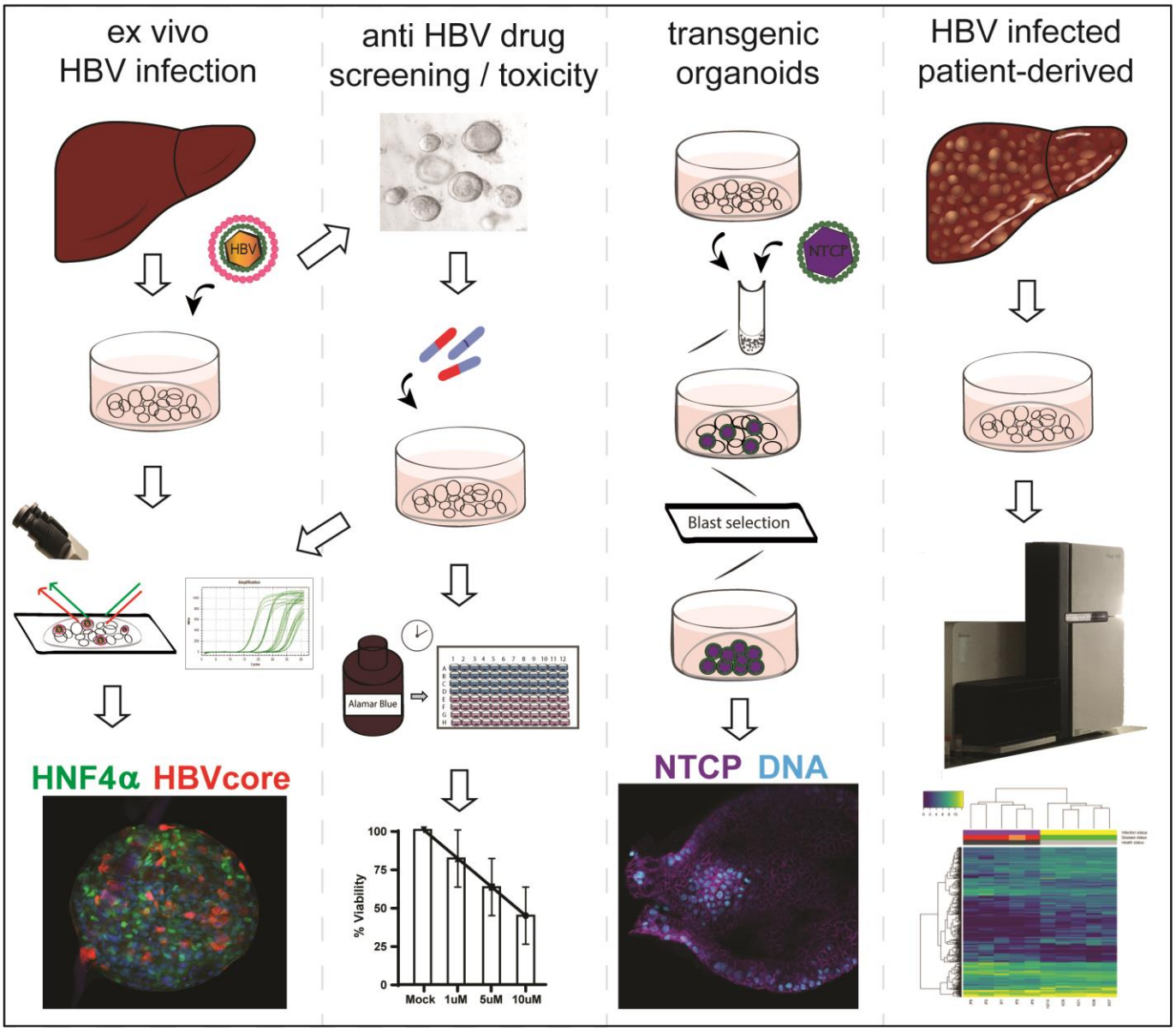

Fig. 6: Schematic of applications of human liver organoids in HBV studies

Materials and Methods

Liver tissue: The Medical Ethical Council of the Erasmus Medical Center approved the use of this material for research purposes, and informed consent was provided from all patients. Biopsies from twelve explanted HBV infected livers and from one HBV infected donor liver were fixed for 24 hours at room temperature in 4% formaldehyde solution (Klinipath) immediately after collection in the operating room. Fixed biopsies were processed according to standard protocol to dehydrate and infiltrate with paraffin wax and subsequent embedding into paraffin blocks. Sections of 4µm were cut using a microtome and mounted on glass microscope slides. After deparaffination according to standard procedure, the tissue slides were stained with haematoxylin and eosin (Haemalum – Mayer's, VWR) according to the manufacturers protocol, dehydrated and mounted for microscopic analysis.

Isolation and culture of human liver organoids: Liver organoids from healthy donors and HBV infected patients were isolated and cultured using the method previously described by Huch et al.(Huch et al., 2015) with minor modifications. In brief, liver specimens (1-2 cm^3) were washed once with DMEM (Sigma) supplemented with 1% FCS and with 0.1% Penicillin Streptomycin (PS, Sigma), minced and incubated at 37°C with the digestion solution (collagenase 2.5mg/ml in EBSS). Incubation was performed for 30 minutes, further mincing and mixing the tissue every 10 minutes. To recover the cells, digestion solution was passed through a 70µM strainer in a 50 ml tube (GreinerBio) and washed with 45ml Advanced DMEM (Gibco) supplemented with 1% PS, 10mM HEPES (Gibco) and 1% GlutaMax (Gibco), henceforth Ad+++. Partially digested tissue was recovered from the strainer and further incubated with TrypLE Express (Thermoscientific) for 15 minutes at 37°C. Cells obtained from the first and second digestion were pooled together and washed twice with Ad+++. After the second centrifugation (200g, 5 minutes) cells were counted, mixed with an appropriate amount of BME solution (2/3 Basement Membrane Extract, Type 2 (Pathclear) diluted with 1/3 Ad+++) and seeded in 25µl drops containing 10000-15000 cells in 48 well suspension plates (GreinerBio). After BME solution had solidified, wells were filled with 250µl of human liver organoid isolation medium consisting Ad+++ supplemented of 1X B27 supplement without retinoic acid (Gibco), 1X N2 supplement (Gibco), 1.25mM N-acetyl-L-cysteine (Sigma), 20% (vol/vol) Rspo-1 conditioned medium(Huch et al., 2013), 1.25% (vol/vol) Wnt3a-conditioned medium(Barker et al., 2010), 10mM nicotinamide (Sigma), 10nM recombinant human (Leu15)-gastrin I (Sigma), 50ng/ml recombinant human EGF (Peprotech), 100ng/ml recombinant human FGF10 (Peprotech), 25ng/ml recombinant human HGF (Peprotech), 10µM Forskolin (Sigma), 5µM A8301 (Tocris), 25ng/ml Noggin (Peprotech)

and 10µM Y27632 Rho Kinase (ROCK) Inhibitor (Sigma). After 1 week, isolation media was changed to human liver expansion media (EM; Ad+++ supplemented of 1X B27 supplement without retinoic acid (Gibco), 1X N2 supplement (Gibco), 1.25mM N-acetyl-L-cysteine (Sigma), 20% (vol/vol) Rspo-1 conditioned medium, 1.25% (vol/vol) Wnt3a-conditioned medium,(Barker et al., 2010) 10mM nicotinamide (Sigma), 10nM recombinant human (Leu15)-gastrin I (Sigma), 50ng/ml recombinant human EGF (Peprotech), 100ng/ml recombinant human FGF10 (Peprotech), 25ng/ml recombinant human HGF (Peprotech), 10µM Forskolin (Sigma) and 5µM A8301 (Tocris)) (Huch et al., 2015).

EM was changed twice a week, and cultures were split every 7-10 days according to organoid density. For passaging (1:4-1:8, depending on growth rate of the culture), organoids were resuspended in 10ml Ad+++, incubated in ice for 10 minutes and collected by centrifugation (5 minutes at 200g). Subsequently, organoids were incubated for 1-2 minutes in TrypLE Express at room temperature and mechanically disrupted by pipetting. After a further wash in Ad+++, cells were resuspended in BME solution and seeded in 24 or 48 wells suspension plates. After BME solution had solidified, wells were filled with 500µl (24 wells) or 250µl (48 wells) of human liver organoid expansion medium.

Hepatic differentiation of liver organoids: Human liver organoid cultures derived from healthy and HBV infected livers were seeded and cultured for 4 days in EM without Wnt3a-conditioned medium supplemented with 25ng/ml of BMP7 (Peprotech). Hepatic differentiation was induced by culturing human liver organoids in differentiation medium (DM; Ad+++ supplemented with 1X B27 supplement without retinoic acid, 1X N2 supplement, 1mM N-acetylcysteine, 10nM recombinant human [Leu15]-gastrin I, 50ng/ml recombinant human EGF, 25ng/ml recombinant human HGF, 0.5µM A83-01, 10µM DAPT (Sigma), 3µM dexamethasone (Sigma), 25ng/ml BMP7 and 100ng/ml recombinant human FGF19 (Peprotech)). Differentiation medium was changed twice a week for 7 days before infection or 10 days before staining for Albumin and HNF4α(Huch et al., 2015). For subsequent downstream analysis the following amounts of organoids are required (Table 4).

Table 4 Recommended starting material quantities

Procedure	Number of wells/ condition	Number of organoids/ well
DNA isolation	1x 24 well plate	≈100-500 organoids/well
RNA isolation	1x 24 well plate	
cccDNA isolation	20-24x 24 well plate	
Immunofluorescence staining	5-10x 24 well plate	

Total RNA isolation and quantitative RT qPCR: RNA extraction was performed starting from 1-2 wells of a 24 wells plate, organoids were collected in 500µl of cell lysis buffer and processed using RealiaPrep RNA Cell Miniprep System (Promega), according to manufacturer's instructions. cDNA synthesis was performed starting from 300-1000ng of RNA using Superscript II Reverse Transcriptase (Life Technologies) kit following manufacturer's protocol for random primer cDNA synthesis. cDNA was diluted 1:5 in nuclease free water and 2µl of the diluted product was used for real time PCR with the following reagents: 5µl of GoTaq qPCR Master Mix (Promega), 2µl of nuclease free water and 1µl of 10mM primer mix. Amplification was performed on the CFX Connect Real-Time PCR Detection System thermocycler (BioRad) using following thermal program starting with 3 minutes at 95°C, followed by 40 cycles of 95°C for 10 seconds and 60°C for 30 seconds. Specificity of the RT-qPCR products was assessed by melting curve analysis. Primers used for real-time qPCR are listed below.

GAPDH Fwd 5'-CAAGAAGGTGGTGAAGCAG-3'; Rev 5'-GCCAAATTCGTTGTCATACC-3'

KRT7 Fwd 5'-CTCCGGAATACCCGGAATGAG-3'; Rev 5'-ATCACAGAGATATTCACGGCTCC-3'

CYP3A4 Fwd 5'-TGTGCCTGAGAACACCAGAG-3'; Rev 5'-GTGGTGGAAATAGTCCCGTG-3'

NTCP Fwd 5'-GCTTTCTGCTGGGTTATGTTCTC-3'; Rev 5'-CATCCAGTCTCCATGCTGACA-3'

HNF4A Fwd 5'-CGTGCTGCTCCTAGGCAATGAC-3'; Rev 5'-ACGGACCTCCCAGCAGCATCT-3'

SOX9 Fwd 5'-GGAAGTCGGTGAAGAACGGG-3'; Rev 5'-TGTTGGAGATGACGTCGCTG-3'

ALBUMIN Fwd 5'-GCGACCATGCTTTTCAGCTC-3'; Rev 5'-GTTGCCTTGGGCTTGTGTTT-3'

LGR5 Fwd 5'-AGGTCTGGTGTGTTGCTGAGG-3'; Rev 5'-TGAAGACGCTGAGGTTGGAAGG-3'

LDLR Fwd 5'-GACGTGGCGTGAACATCTG-3'; Rev 5'-CTGGCAGGCAATGCTTTGG-3'

PCSK9 Fwd 5'-AGGGGAGGACATCATTGGTG-3'; Rev 5'-CAGGTTGGGGGTCAGTACC-3'

Gene expression levels were calculated using the 2ΔCt method, whereas fold increase was calculated using the 2ΔΔCt (Schmittgen & Livak, 2008). GAPDH was used as housekeeping control.

Immunofluorescence and image analysis: Human liver organoids were collected and washed three times to with cold Ad+++ to remove BME, then fixed with 4% paraformaldehyde for 30 minutes in ice and permeabilized using 0.3% (HBcAg, HNF4α and NTCP) or 1% (Albumin) Triton X-100 (Sigma) in PBS for 30 minutes at room temperature. For HBsAg staining cells were fixed and permeabilized in 100% Acetone. Specimens were incubated for 2h at room temperature in PBS plus 10% BSA (Roche)

and 0.5% FCS (HBsAg) or PBS plus 0.5% FCS, 0.3% triton, 1% BSA 1%DMSO (Albumin, HBcAg, HNF4α and SLC10A1). Following blocking, human liver organoids were incubated overnight with primary antibodies (mouse anti-HBcAg, mouse anti- HBsAg (ThermoScientific), goat anti-Albumin, rabbit anti-HNF4α (Santa Cruz Biotechnology) and rabbit anti-SLC10A1 (NTCP, Sigma) diluted in PBS + 10% blocking buffer. After extensive washing, human liver organoids were stained with appropriate Alexa Fluor dye-conjugated secondary antibodies (Life Technologies). Nuclei were stained with Hoechst33342 (Molecular Probes). Immunofluorescence images were acquired using a confocal microscope (Leica, SP5). Images were analyzed and processed using Leica LAS AF Lite software (Leica SP5 confocal). All phase contrast pictures were acquired using a Leica DMIL microscope and a DFC420C camera.

Production of HBV virus and HBV infection: HepG2.2.15 cells, a HepG2 derived cells line stably transfected with full length HBV (kindly provided by Prof. Bart Haagmans, Erasmus MC) were cultured in DMEM medium (Gibco) supplemented with 10% fetal bovine serum (Gibco) and 1% penicillin/streptomycin. For virus production, $3x10^6$ cells were plated in collagen coated 10cm plates, cultured in supplemented DMEM until confluency and subsequently in Ad+++ for 4 days. The supernatant of HepG2.2.15 cells was then collected, filtered and concentrated using the PEG Virus Precipitation Kit (Abcam) following the manufacturer's instructions. Precipitated virus was aliquoted and stored at -80°C until use. Human serum was obtained from residual samples from HBV infected individuals attending Erasmus MC for routine clinical activity. As negative control, an aliquot of the virus equivalent to the inoculum was inactivated by incubation at 100°C for 30 minutes. Human liver organoids were resuspended using either active virus or heat inactivated control at an MOI of 1-10 * 10^3 copies HBV DNA/organoid, transferred to 24 wells plate and centrifuged for 1h at 600g. Following spinoculation, plates were incubated at 37°C for 5h and then seeded in BME following the culturing protocol. After BME solution has solidified, liver organoids were maintained in EM for 16h, washed 4 times with Ad+++ and cultured EM or DM as indicated.

Detection of HBV DNA and RNA: DNA was extracted from culture supernatants using the QIAamp MinElute Virus Spin Kit following manufacturer's instructions. DNA extracted from supernatant and cDNA obtained from reverse transcription of intracellular DNA (see section 9 for details) were analyzed in duplicate using a TaqMan based qPCR assay. For each reaction, a 25ul mixture was prepared containing 2.5µl 10X Buffer, 1.75µl 25mM MgCl2, 1µl 10mM dNTPs, 1U of Platinum Taq, 0.125µl of 100µM forward (5'-GCAACTTTTTCACCTCTGCCT A-3') and reverse primer (5'-

AGTAACTCCACAGTAGCTCCAAATT-3'), 0.075µl of 50µM probe (FAM-TTCAAGCCTCCAAGCTGTGCCTTGGGTGGC-TAMRA), and 7.5µl (DNA) or 4µl (cDNA) of template. Each PCR reaction included a standard curve made of dilutions of a plasmid containing the full-length HBV genome ranging from 4 to $4x10^5$ copies of plasmid. Beta-2-microglobulin was used as housekeeping control for expression analysis of cDNA samples (B2M Fwd 5'-AGCGTACTCCAAAGATTCAGGTT-3', B2M Rev 5'-ATGATGCTGCTTACATGTCTCGAT-3', B2M probe FAM-TCCATCCGACATTGAAGTTGACTTACTG-BHQ1).

Detection of pol and HBX transcripts was performed using a previously published nested PCR protocol (Wong et al., 2011).

Isolation and detection of HBV cccDNA from infected liver organoids: HBV cccDNA was isolated from HBV and HI (negative control) infected human liver organoids by a previously described alkali lysis plasmid DNA isolation protocol with a minor modification (Yang, Mason, & Summers, 1996). Briefly, Human liver organoids were collected on day 8 post infection incubated on ice for 10-20 mins and washed with Ad+++ to remove the BME. After centrifugation (5 mins at 1000rpm) organoids were treated with TrypLE Express and incubated for 30-50 sec at room temperature. Organoids were washed with PBS and collected by centrifugation (5 mins at 1000rpm), resuspended with 800µl of ice-cold cell lysis buffer (1mM EDTA (pH 8.0), 5mM Tris: HCl (pH 7.5) and 0.05% Nonidet P-40). After 10 min incubation on ice, an equal volume of alkali lysis buffer (0.1M NaOH, 6% SDS) was added and the solution was incubated for 30 mins at 37°C. DNA was neutralized by adding 3M potassium acetate (pH 5.0) to a final concentration of 0.6M and centrifuged for 5 mins at 12000 rpm. The supernatant was extracted two times with phenol followed by extraction with butanol: isopropanol (7:3) for removal of residual phenol. Subsequently, the DNA was precipitated with 1ml 100% ethanol, 400µl 7.5M ammonium acetate and 1µl 20mg/ml glycogen overnight at -80°C. Next day, the cccDNA sample was spun down for 30 mins at 4°C, 14000 rpm and washed with 70% ethanol. After spinning the samples for 15 mins at 4°C, 14000 rpm, the pellet was resuspended in 50µl of nuclease free water.

To remove the chromosomal DNA or any linear HBV DNA, 25µl of the isolated HBV cccDNA, HBV plasmid (positive control) and HBV DNA from inoculum was digested with plasmid-safe DNase (Epicentre, E3101K, Madison, WI). According to the manufacturer's protocol, the samples were digested for 1 hr at 37°C followed by 30 mins of heat inactivation at 70°C. The digested samples were purified once with phenol: chloroform: isoamyalcohol (Sigma-Aldrich) followed by treatment

chloroform: isoamylalcohol (24:1), cccDNA was precipitated with 20ul 3M NaAC (pH 5.2), 1ul glycogen (20mg/ml), 1ml 100% ethanol and washed as described above.

For quantification of cccDNA a TaqMan based qPCR was performed, whereby for each reaction 20µl reaction-mix was prepared containing 4.2µl of the diluted cccDNA, 10µl LightCycler®480 Probes Master (Roche), 1µM primer mix (Fwd 5'-GTCTGTGCCTTCTCATCTGC-3'; Rev 5'-AGTAACTCCACAGTAGCTCCAAATT-3'), 0.2µM probe (FAM-TTCAAGCCTCCAAGCTGTGCCTTGGGTGGC-BHQ1) and 4% DMSO. qPCR was carried out using a previously published protocol 95°C for 10 min, followed by 50 cycles of 95°C for 15 s, and 61°C for 1 min (Winer et al., 2017).

Infection with HBV generated from organoids: the supernatant produced by infected organoids at 4-8 days post infection was collected and concentrated using Amicon Ultra-15 100K (Milipore). Human liver organoids were resuspended using either concentrated HBV virus or HI control. After an hour of spinoculation at 32°C 600g, plate was incubated at 37°C overnight and then washed & seeded in BME following the HBV infection and culturing protocol.

Cell culture: HepG2 and HepG2.215 cells were cultured in DMEM medium (Gibco) supplemented with 10% fetal bovine serum (Gibco) and 1% penicillin/streptomycin and incubated in 5% CO2 at 37°C.

Viability assays: HepG2 cells with cell density of 2×10^4 cells/ml were seeded in 24-well plate with DMEM high-glucose media supplemented with fetal bovine serum (10% v/v) and penicillin/streptomycin (1% v/v) and incubated in 5% CO2 at 37 °C for overnight. Human liver organoids seeded from healthy donor or HBV infected patient livers were split in the ratio of 1:10, seeded in 20µl BME 3D culture in 48- well plates and differentiated as described above. 10 days post differentiation for human liver organoids and 24 hrs post seeding of the HepG2 cells they were treated with different concentrations of Fialuridine (Cayman, 15867-1) or Tenofovir disproxil fumarate (Sigma, SML1794) (1-20µM) or the vehicle control. At different time points (2-10 days) post treatment, organoid viability was measured using the AlamarBlue viability assay (alamarBlue™ Invitrogen DAL1025, 1:10 in DM) according to manufacturer's instructions. Briefly, treatment DM medium was removed from wells and 10% Alamar blue with DM was added to each well and incubated for 4 hours (organoids) or 2 hours (HepG2 cells) at 37°C before absorbance readings were taken at 570 and 600 nm. The results were normalized to control vehicle treated differentiated organoids. The lower limit of quantitation of the assay was determined by values obtained from BME

without organoids and is represented by dotted line in figure panels. Each treatment condition was repeated at least 3 times and readings were done in duplicate. Cell imaging was performed after each Alamar blue assay.

3' mRNA sequencing: For each RNA preparation, 2 wells of organoids in expansion phase were collected in Trizol reagent (Sigma) 4-5 days after splitting. RNA was extracted according to manufacturer's instruction and resuspended in 30µl of nuclease free water. Total RNA was quantitated (ND1000 Spectrophotometer – PEQLAB). Samples were diluted accordingly to a mean concentration of approximately 100-150ng/µl and their quality assessed on a Bioanalyzer (Agilent Technologies) using the Agilent RNA 6000 Nano Kit reagents and protocol (Agilent Technologies). RNA samples were processed for library preparation using the 3' mRNA-Seq Library Prep Kit Protocol for Ion Torrent (QuantSeq-LEXOGEN™, Vienna, Austria), according to manufacturer's instructions. Briefly, up to 500ng from each RNA sample were used for first strand synthesis. The RNA was subsequently removed and 2nd strand synthesis was initiated by a random primer, containing Ion Torrent compatible linker sequences and appropriate in-line barcodes. 2nd strand synthesis was followed by magnetic bead-based purification and the resulting library was PCR-amplified for 14 cycles and re-purified. Library quality and quantity was assessed on a Bioanalyzer using the DNA High Sensitivity Kit reagents and protocol (Agilent Technologies). The quantified libraries were pooled together at a final concentration of 100pM. The pools were templated and enriched on an Ion Proton One Touch system. Templating was performed using the Ion PI™ Hi-Q™ OT2 200 Kit (Thermo Fisher Scientific), followed by sequencing using the Ion PI™ Hi-Q™ Sequencing 200 Kit on Ion Proton PI™ V2 chips (Thermo Fisher Scientific), an Ion Proton™ System, according to the manufacturer's instructions.

Short read mapping: The Quant-Seq FASTQ files obtained from Ion Proton sequencing were mapped on the UCSC hg19 reference genome using a two-phase mapping procedure. Firstly, the short reads were mapped using tophat2(Kim et al., 2013), with the following non-default settings: --read-mismatches 3 --read-gap-length 3 --read-edit-dist 3 --no-novel-juncs, other settings at default. Additional transcript annotation data for the hg19 genome from Illumina iGenomes (http://cufflinks.cbcb.umd.edu/igenomes.html) was also provided to tophat2 for guidance. Next, the reads which remained unmapped were converted back to FASTQ files using bam2fastq from the BEDTools (Quinlan & Hall, 2010) suite and submitted to a second round of mapping using Bowtie2 (Langmead & Salzberg, 2012) against the hg19 genome with the --local and --very-sensitive-local

switches turned on. All resulting BAM files were visualized in the UCSC Genome Browser using BEDTools and tools provided by the UCSC Genome Browser toolkit.

Statistical analysis of Quant-Seq data: The resulting Quant-Seq BAM files were analyzed with the Bioconductor package metaseqR(Moulos & Hatzis, 2015) which has built-in support for Quant-Seq data. Briefly, the raw BAM files, one for each organoid sample, were summarized to a 3' UTR read counts table from Ensembl longest (dominant) transcripts (version 90). The original 3' UTR regions were extended 500bp upstream and downstream to accommodate the variable read length of Ion Proton reads. In the resulting read counts table, each row represented one 3' UTR region, each column one Quant-Seq sample and each cell the corresponding read counts associated with each row and column. The final 3' UTR read counts table was normalized for inherent systematic or experimental biases using the Bioconductor package DESeq (Anders, Reyes, & Huber, 2012) after removing areas that had zero counts over all the Quant-Seq samples. Prior to the statistical testing procedure, the 3' UTR read counts were filtered for possible artifacts that could affect the subsequent statistical testing procedures. 3' UTR areas presenting any of the following were excluded from further analysis: i) 3' UTR areas corresponding to genes smaller than 500bp, ii) 3' UTRs with read counts below the median read counts of the total normalized count distribution. Similar expression thresholds (e.g. the median of the count distribution) have been previously used in the literature(Mokry et al., 2012), where the authors use the median RPKM value instead of normalized counts), iii) 3' UTR areas corresponding to genes with the following Ensembl biotypes: rRNA, TR_V_pseudogene, TR_J_pseudogene, IG_C_pseudogene, IG_J_pseudogene, IG_V_pseudogene. The remaining 3' UTR counts table after filter application was subjected to differential expression analysis for the appropriate contrasts using the PANDORA algorithm implemented in metaseqR. 3' UTR areas (and their corresponding genes) presenting a PANDORA p-value less than 0.05 and fold change (for each contrast) greater than 1 or less than -1 in log2 scale were considered as differentially expressed.

Clustering analysis: Hierarchical clustering was performed using the Euclidean distance and complete linkage for the construction of the dendrograms. The expression values used to generate the heatmap were DESeq-normalized read counts in log2 scale. Multidimensional scaling was performed using the Spearman correlation distance metric on the gene expression matrix using DESeq-normalized read counts in log2 scale. All calculations and visualizations were performed using facilities from the R language. All analysis scripts and logs of the analysis pipelines are available upon request.

Gene Ontology and Pathway analysis: Gene Ontology (GO) enrichment and biochemical pathway analysis was performed using GeneCodis(Tabas-Madrid, Nogales-Cadenas, & Pascual-Montano, 2012). For the GeneCodis GO and pathway analysis the 361 iP "Signature" genes were used

Generation of the lentiviral vectors and transduction of liver organoids: A gene block fragment encoding human NTCP was designed based on the reference sequence retrieved from NCBI nucleotide database (NM_003049.3). A 3X Flag PCR fragment including NTCP coding sequence was amplified using the NTCP_FWD (CACCATGGATTACAAGGATGACGACGATAAGGATTACAAGGATGACGACGATAAGGATTACAAGGATGACGACGATAAGATGGAGGCCCACAACGCGTCTgcccca) and NTCP_REV (TTACTAGGCTGTGCAAGGGGAGCA) primers and cloned in the pENTR/D-TOPO entry vector (Invitrogen) following manufacturer's instructions.

A pENTR/D-TOPO vector harboring a competent full-length copy of HBV (1.3 wt genomes) was generated using a Gibson Assembly protocol. Two fragments encompassing 1.3 times the wt HBV genome were purified using the QIAquick PCR Purification Kit (Qiagen) after PCR using the following primer pairs: VectorFwd (5'-caaaaaagcaggctccgcggccgcccccttcacGGACGACCCTTCTCGGGG-3')/MiddleRev (5'-gagaagtccaccacgAGTCTAGACTCTGCGGTATTGTGAG-3') and MiddleFwd (5'-cgcagagtctagactCGTGGTGGACTTCTCTCAATTTTC-3')/ VectorRev (5'-tgccaactttgtacaagaaagctgggtcggAGGGGCATTTGGTGGTCTATAAG-3'). The HepG2.2.15 DNA was used as template for the PCR: An empty pENTR/D-TOPO was cut with NotI and BssHI and gel purified using QIAquick Gel Extraction Kit (Qiagen). After purification, the entry vector and the PCR fragments were assembled using the Gibson Assembly Master Mix (New England BioLabs), following manufacturer's instructions.

To generate lentiviral constructs, the fragments cloned into entry vectors were transferred to a lentiviral expression destination vector (pLenti6/V5-DEST Gateway Vector, Invitrogen), using the Gateway technology (Invitrogen). The full-length HBV pLenti6/V5-DEST vector was further modified in order to remove the CMV promoter. The vector was digested with two restriction enzymes flanking the CMV promoter, ClaI and PstI (New England Biolabs), and purified from gel using QIAquick Gel Extraction Kit. After filling end gaps using Klenow polymerase (New England Biolabs), plasmids were ligated and transformed in One Shot® Stbl3™ Chemically Competent E. coli (Invitrogen). All HBV and NTCP lentiviral vectors were sequenced to verify vector structure and integrity of open reading frames.

The lentiviral constructs were generated using the ViraPower Kit (Invitrogen) and 293FT cells, following manufacturer's protocol. Briefly, one day prior transfection, $3x10^5$ cells were plated in 10cm dishes in DMEM + 10% FCS. The following day, DMEM was replaced with 5ml of Opti MEM I (Invitrogen) and cells were transfected with 9µg of the ViraPower Packaging Mix and 3µg of the pLenti6/V5-DEST Gateway Vector using Lipofectamine (Invitrogen). The day after transfection media was changed to DMEM + 10% FCS. Cell supernatant containing the lentiviral particles was collected 60 and 72 hours after transfection, filtered with a 0.42µm filter, aliquoted and stored at -80°C.

Early passage (passage 0 to 3) human liver organoids were collected in cold Ad+++ and incubate for 10 minutes in ice to remove BME. After centrifugation (5 minutes at 200g), organoids were resuspended in TrypLE Express and incubated until single cells were >80%. Cells were collected by centrifugation (5 minutes at 200g), resuspended in 1ml of lentiviral harvest and divided over 4 wells of a 48 wells plate. Plates were centrifugated for 1h at 600g and then incubated for 5h at 37°C. Afterwards, cells were collected by centrifugation (5 minutes at 200g), resuspended in BME solution and plated. After BME has solidified, wells were filled with EM supplemented with 25ng/ml Noggin and 10µM Y27632. Four days after infection medium was changed to EM supplemented with 25ng/ml Noggin and 10µM Rho Kinase (ROCK) Inhibitor Y27632 and 5ug/ml blasticidin. Organoids were kept under selection for 7 days and then media was changed to regular EM. Once selected organoids have recovered, cultures were splitted to remove dead cells and cultured according to the regular protocol. Parallel infections were performed using HepG2 cells and the same lentiviral constructs in order to generate control cell lines.

To determine NTCP functionality following transduction with NTCP lentiviral vector, parental and selected NTCP transduced organoids were cultured in EM or EM supplemented with different concentrations of Aruvastatin and Rosuvastatin for 12h. Organoids from 2 wells of a 24 wells plate were collected in 500µl of cell lysis buffer and processed using RealiaPrep RNA Cell Miniprep System (Promega), according to manufacturer's instructions.

To determine HBV production following transduction with full length HBV lentiviral vector, supernatant and cells from transduced cultures were collected at different time points after completion of blasticidin selection. Presence of viral DNA in the supernatant and cellular associated viral RNA was assessed using the real time protocol detailed in section 11. Presence of HBsAg in organoid supernatant was assessed using the MonaLisa Kit (Promega) according to manufacturer's instructions.

Data availability:

Sequencing data that support the findings of this study have been deposited in GEO with the accession code GSE 126798.

Statistical analysis:

The data were first analyzed by ANOVA, and then each pair was compared through Dunnett's multiple comparisons test. A value of $p < 0.05$ was considered statistically significant. Data are shown as mean ± SD of at least 3 replicate treatments $*P < 0.05$; $**P < 0.01$. The data were analyzed and graphs were depicted by GraphPad Prism software 5 (GraphPad Software, La Jolla, CA, USA). Obtained data from drug screening of infected organoid have 2-8 technical replicates for each donor. Thus, the obtained data from each donor were analyzed by ANOVA separately.

Acknowledgments

We would like to thank Vaggelis Harokopos for NGS and Karien Hamer for technical support.

TM received funding from the European Research Council (ERC) under the European Union's Seventh Framework Programme (FP/2007-2013)/ERC STG 337116 Trxn-PURGE, Dutch AIDS Fonds grants 2014021 and 2016014, and Erasmus MC mRACE research grant.

Conflicts of interest

EDC received funding from Bristol Meyers Squibb (Partnering for the cure program).

Author Contributions

EDC, SR, FC, MMK, AB, SGR, TWK, FP and TM carried out the experiments and performed data analysis. PM, CK, RJP, and PH performed RNAseq and gene expression analysis. MMA, LVDL, JMNI, CB provided tissue samples and serum from HBV infected patients. FP, MMA, LVDL, CB, HG, MH, SFB, SR, SGR, RV, HC, and provided expertise, material and contributed to the writing of the manuscript. EDC, FC, RV, PH and TM conceived the study and wrote the manuscript. All authors read and approved the final manuscript.

References

Allain, C., Angenard, G., Clement, B., & Coulouarn, C. (2016). Integrative Genomic Analysis Identifies the Core Transcriptional Hallmarks of Human Hepatocellular Carcinoma. *Cancer Res, 76*(21), 6374-6381. DOI: https://doi.org/10.1158/0008-5472.CAN-16-1559. PMCID: PMC5660733

Allweiss, L., & Dandri, M. (2016). Experimental in vitro and in vivo models for the study of human hepatitis B virus infection. *Journal of hepatology, 64*(1), S17-S31. DOI: https://doi.org/10.1016/j.jhep.2016.02.012.

Anders, S., Reyes, A., & Huber, W. (2012). Detecting differential usage of exons from RNA-seq data. *Genome Res, 22*(10), 2008-2017. DOI: https://doi.org/10.1101/gr.133744.111. PMCID: PMC3460195

Ashida, R., Okamura, Y., Ohshima, K., Kakuda, Y., Uesaka, K., Sugiura, T., . . . Yamaguchi, K. (2017). CYP3A4 Gene Is a Novel Biomarker for Predicting a Poor Prognosis in Hepatocellular Carcinoma. *Cancer Genomics Proteomics, 14*(6), 445-453. DOI: https://doi.org/10.21873/cgp.20054. PMCID: PMC6070324

Barker, N., Huch, M., Kujala, P., van de Wetering, M., Snippert, H. J., van Es, J. H., . . . Clevers, H. (2010). Lgr5(+ve) stem cells drive self-renewal in the stomach and build long-lived gastric units in vitro. *Cell Stem Cell, 6*(1), 25-36. DOI: https://doi.org/10.1016/j.stem.2009.11.013.

Cancer Genome Atlas Research Network. Electronic address, w. b. e., & Cancer Genome Atlas Research, N. (2017). Comprehensive and Integrative Genomic Characterization of Hepatocellular Carcinoma. *Cell, 169*(7), 1327-1341 e1323. DOI: https://doi.org/10.1016/j.cell.2017.05.046.

Chen, Y., Zhao, Z. X., Huang, F., Yuan, X. W., Deng, L., & Tang, D. (2019). MicroRNA-1271 functions as a potential tumor suppressor in hepatitis B virus-associated hepatocellular carcinoma through the AMPK signaling pathway by binding to CCNA1. *J Cell Physiol, 234*(4), 3555-3569. DOI: https://doi.org/10.1002/jcp.26955.

El-Serag, H. B. (2012). Epidemiology of viral hepatitis and hepatocellular carcinoma. *Gastroenterology, 142*(6), 1264-1273 e1261. DOI: https://doi.org/10.1053/j.gastro.2011.12.061. PMCID: PMC3338949

Fattovich, G., Bortolotti, F., & Donato, F. (2008). Natural history of chronic hepatitis B: special emphasis on disease progression and prognostic factors. *J Hepatol, 48*(2), 335-352. DOI: https://doi.org/10.1016/j.jhep.2007.11.011.

Fujimoto, A., Totoki, Y., Abe, T., Boroevich, K. A., Hosoda, F., Nguyen, H. H., . . . Nakagawa, H. (2012). Whole-genome sequencing of liver cancers identifies etiological influences on mutation patterns and recurrent mutations in chromatin regulators. *Nat Genet, 44*(7), 760-764. DOI: https://doi.org/10.1038/ng.2291.

Gao, W., Kondo, Y., Shen, L., Shimizu, Y., Sano, T., Yamao, K., . . . Sekido, Y. (2008). Variable DNA methylation patterns associated with progression of disease in hepatocellular carcinomas. *Carcinogenesis, 29*(10), 1901-1910. DOI: https://doi.org/10.1093/carcin/bgn170.

Huang, J., Deng, Q., Wang, Q., Li, K. Y., Dai, J. H., Li, N., . . . Han, Z. G. (2012). Exome sequencing of hepatitis B virus-associated hepatocellular carcinoma. *Nat Genet, 44*(10), 1117-1121. DOI: https://doi.org/10.1038/ng.2391.

Huch, M., Dorrell, C., Boj, S. F., van Es, J. H., Li, V. S., van de Wetering, M., . . . Clevers, H. (2013). In vitro expansion of single Lgr5+ liver stem cells induced by Wnt-driven regeneration. *Nature, 494*(7436), 247-250. DOI: https://doi.org/10.1038/nature11826. PMCID: PMC3634804

Huch, M., Gehart, H., van Boxtel, R., Hamer, K., Blokzijl, F., Verstegen, M. M., . . . Clevers, H. (2015). Long-term culture of genome-stable bipotent stem cells from adult human liver. *Cell, 160*(1-2), 299-312. DOI: https://doi.org/10.1016/j.cell.2014.11.050. PMCID: PMC4313365

Iwamoto, M., Watashi, K., Tsukuda, S., Aly, H. H., Fukasawa, M., Fujimoto, A., . . . Wakita, T. (2014). Evaluation and identification of hepatitis B virus entry inhibitors using HepG2 cells overexpressing a membrane transporter NTCP. *Biochem Biophys Res Commun, 443*(3), 808-813. DOI: https://doi.org/10.1016/j.bbrc.2013.12.052.

Ji, X., Zhang, Q., Du, Y., Liu, W., Li, Z., Hou, X., & Cao, G. (2014). Somatic mutations, viral integration and epigenetic modification in the evolution of hepatitis B virus-induced hepatocellular carcinoma. *Curr Genomics, 15*(6), 469-480. DOI: https://doi.org/10.2174/1389202915666141114213833. PMCID: PMC4311391

Jiang, Z., Jhunjhunwala, S., Liu, J., Haverty, P. M., Kennemer, M. I., Guan, Y., . . . Zhang, Z. (2012). The effects of hepatitis B virus integration into the genomes of hepatocellular carcinoma patients. *Genome Res, 22*(4), 593-601. DOI: https://doi.org/10.1101/gr.133926.111. PMCID: PMC3317142

Kaneko, S., Kakinuma, S., Asahina, Y., Kamiya, A., Miyoshi, M., Tsunoda, T., . . . Watanabe, M. (2016). Human induced pluripotent stem cell-derived hepatic cell lines as a new model for host interaction with hepatitis B virus. *Sci Rep, 6*, 29358. DOI: https://doi.org/10.1038/srep29358. PMCID: PMC4937433

Kim, D., Pertea, G., Trapnell, C., Pimentel, H., Kelley, R., & Salzberg, S. L. (2013). TopHat2: accurate alignment of transcriptomes in the presence of insertions, deletions and gene fusions. *Genome Biol, 14*(4), R36. DOI: https://doi.org/10.1186/gb-2013-14-4-r36. PMCID: PMC4053844

Langmead, B., & Salzberg, S. L. (2012). Fast gapped-read alignment with Bowtie 2. *Nat Methods, 9*(4), 357-359. DOI: https://doi.org/10.1038/nmeth.1923. PMCID: PMC3322381

Lee, E.-W., Lai, Y., Zhang, H., & Unadkat, J. D. (2006). Identification of the Mitochondrial Targeting Signal of the Human Equilibrative Nucleoside Transporter 1 (hENT1) IMPLICATIONS FOR INTERSPECIES DIFFERENCES IN MITOCHONDRIAL TOXICITY OF FIALURIDINE. *Journal of Biological Chemistry, 281*(24), 16700-16706. DOI: https://doi.org/10.1074/jbc.M513825200.

March, S., Ramanan, V., Trehan, K., Ng, S., Galstian, A., Gural, N., . . . Bhatia, S. N. (2015). Micropatterned coculture of primary human hepatocytes and supportive cells for the study of hepatotropic pathogens. *Nat Protoc, 10*(12), 2027-2053. DOI: https://doi.org/10.1038/nprot.2015.128. PMCID: PMC5867906

McKenzie, R., Fried, M. W., Sallie, R., Conjeevaram, H., Di Bisceglie, A. M., Park, Y., . . . Luciano, C. (1995). Hepatic failure and lactic acidosis due to fialuridine (FIAU), an investigational nucleoside analogue for chronic hepatitis B. *New England Journal of Medicine, 333*(17), 1099-1105. DOI: https://doi.org/10.1056/NEJM199510263331702.

Mokry, M., Hatzis, P., Schuijers, J., Lansu, N., Ruzius, F. P., Clevers, H., & Cuppen, E. (2012). Integrated genome-wide analysis of transcription factor occupancy, RNA polymerase II binding and steady-state RNA levels identify differentially regulated functional gene classes. *Nucleic Acids Res, 40*(1), 148-158. DOI: https://doi.org/10.1093/nar/gkr720. PMCID: PMC3245935

Moulos, P., & Hatzis, P. (2015). Systematic integration of RNA-Seq statistical algorithms for accurate detection of differential gene expression patterns. *Nucleic Acids Res, 43*(4), e25. DOI: https://doi.org/10.1093/nar/gku1273. PMCID: PMC4344485

Nie, Y. Z., Zheng, Y. W., Miyakawa, K., Murata, S., Zhang, R. R., Sekine, K., . . . Taniguchi, H. (2018). Recapitulation of hepatitis B virus-host interactions in liver organoids from human induced pluripotent stem cells. *EBioMedicine, 35*, 114-123. DOI: https://doi.org/10.1016/j.ebiom.2018.08.014. PMCID: PMC6156717

Paradis, V., Bieche, I., Dargere, D., Laurendeau, I., Laurent, C., Bioulac Sage, P., . . . Bedossa, P. (2003). Molecular profiling of hepatocellular carcinomas (HCC) using a large-scale real-time RT-PCR approach: determination of a molecular diagnostic index. *Am J Pathol, 163*(2), 733-741. DOI: https://doi.org/10.1016/S0002-9440(10)63700-5. PMCID: PMC1868199

Protzer, U. (2017). The bumpy road to animal models for HBV infection. *Nature Reviews Gastroenterology & Hepatology, 14*(6), 327-328. DOI: https://doi.org/10.1038/nrgastro.2017.44.

Quinlan, A. R., & Hall, I. M. (2010). BEDTools: a flexible suite of utilities for comparing genomic features. *Bioinformatics, 26*(6), 841-842. DOI: https://doi.org/10.1093/bioinformatics/btq033. PMCID: PMC2832824

Sagnelli, E., Macera, M., Russo, A., Coppola, N., & Sagnelli, C. (2019). Epidemiological and etiological variations in hepatocellular carcinoma. *Infection*, 1-11. DOI: https://doi.org/10.1007/s15010-019-01345-y.

Sakurai, F., Mitani, S., Yamamoto, T., Takayama, K., Tachibana, M., Watashi, K., . . . Mizuguchi, H. (2017). Human induced-pluripotent stem cell-derived hepatocyte-like cells as an in vitro model of human hepatitis B virus infection. *Sci Rep, 7*, 45698. DOI: https://doi.org/10.1038/srep45698. PMCID: PMC5379564

Sartorius, K., Makarova, J., Sartorius, B., An, P., Winkler, C., Chuturgoon, A., & Kramvis, A. (2019). The Regulatory Role of MicroRNA in Hepatitis-B Virus-Associated Hepatocellular Carcinoma (HBV-HCC) Pathogenesis. *Cells, 8*(12), 1504. DOI: https://doi.org/10.3390/cells8121504. PMCID: PMC6953055

Schmittgen, T. D., & Livak, K. J. (2008). Analyzing real-time PCR data by the comparative C(T) method. *Nat Protoc, 3*(6), 1101-1108. DOI: https://doi.org/10.1038/nprot.2008.73.

Shibata, T., & Aburatani, H. (2014). Exploration of liver cancer genomes. *Nat Rev Gastroenterol Hepatol, 11*(6), 340-349. DOI: https://doi.org/10.1038/nrgastro.2014.6.

Sung, W. K., Zheng, H., Li, S., Chen, R., Liu, X., Li, Y., . . . Luk, J. M. (2012). Genome-wide survey of recurrent HBV integration in hepatocellular carcinoma. *Nat Genet, 44*(7), 765-769. DOI: https://doi.org/10.1038/ng.2295.

Tabas-Madrid, D., Nogales-Cadenas, R., & Pascual-Montano, A. (2012). GeneCodis3: a non-redundant and modular enrichment analysis tool for functional genomics. *Nucleic Acids Res, 40*(Web Server issue), W478-483. DOI: https://doi.org/10.1093/nar/gks402. PMCID: PMC3394297

Tao, R., Li, J., Xin, J., Wu, J., Guo, J., Zhang, L., . . . Li, L. (2011). Methylation profile of single hepatocytes derived from hepatitis B virus-related hepatocellular carcinoma. *PLoS One, 6*(5), e19862. DOI: https://doi.org/10.1371/journal.pone.0019862. PMCID: PMC3100314

Thomas, E., & Liang, T. J. (2016). Experimental models of hepatitis B and C - new insights and progress. *Nat Rev Gastroenterol Hepatol, 13*(6), 362-374. DOI: https://doi.org/10.1038/nrgastro.2016.37. PMCID: PMC5578419

Winer, B. Y., Huang, T. S., Pludwinski, E., Heller, B., Wojcik, F., Lipkowitz, G. E., . . . Ploss, A. (2017). Long-term hepatitis B infection in a scalable hepatic co-culture system. *Nat Commun, 8*(1), 125. DOI: https://doi.org/10.1038/s41467-017-00200-8. PMCID: PMC5527081

Wong, D. K., Huang, F. Y., Lai, C. L., Poon, R. T., Seto, W. K., Fung, J., . . . Yuen, M. F. (2011). Occult hepatitis B infection and HBV replicative activity in patients with cryptogenic cause of hepatocellular carcinoma. *Hepatology, 54*(3), 829-836. DOI: https://doi.org/10.1002/hep.24551.

Xia, Y., Carpentier, A., Cheng, X., Block, P. D., Zhao, Y., Zhang, Z., . . . Liang, T. J. (2017). Human stem cell-derived hepatocytes as a model for hepatitis B virus infection, spreading and virus-host interactions. *J Hepatol, 66*(3), 494-503. DOI: https://doi.org/10.1016/j.jhep.2016.10.009. PMCID: PMC5316493

Xiang, C., Du, Y., Meng, G., Yi, L. S., Sun, S., Song, N., . . . Yi, Z. (2019). Long-term functional maintenance of primary human hepatocytes in vitro. *Science, 364*(6438), 399-402. DOI: https://doi.org/10.1126/science.aau7307.

Yamaguchi, M. (2015). Involvement of regucalcin as a suppressor protein in human carcinogenesis: insight into the gene therapy. *J Cancer Res Clin Oncol, 141*(8), 1333-1341. DOI: https://doi.org/10.1007/s00432-014-1831-z.

Yan, H., Zhong, G., Xu, G., He, W., Jing, Z., Gao, Z., . . . Li, W. (2012). Sodium taurocholate cotransporting polypeptide is a functional receptor for human hepatitis B and D virus. *Elife, 1*, e00049. DOI: https://doi.org/10.7554/eLife.00049. PMCID: PMC3485615

Yang, W., Mason, W. S., & Summers, J. (1996). Covalently closed circular viral DNA formed from two types of linear DNA in woodchuck hepatitis virus-infected liver. *J Virol, 70*(7), 4567-4575. PMCID: PMC190393

Zhang, X.-D., Wang, Y., & Ye, L.-H. (2014). Hepatitis B virus X protein accelerates the development of hepatoma. *Cancer biology & medicine, 11*(3), 182-190. DOI: https://doi.org/10.7497/j.issn.2095-3941.2014.03.004. PMCID: PMC4197427

Figure 1 - figure supplement 1

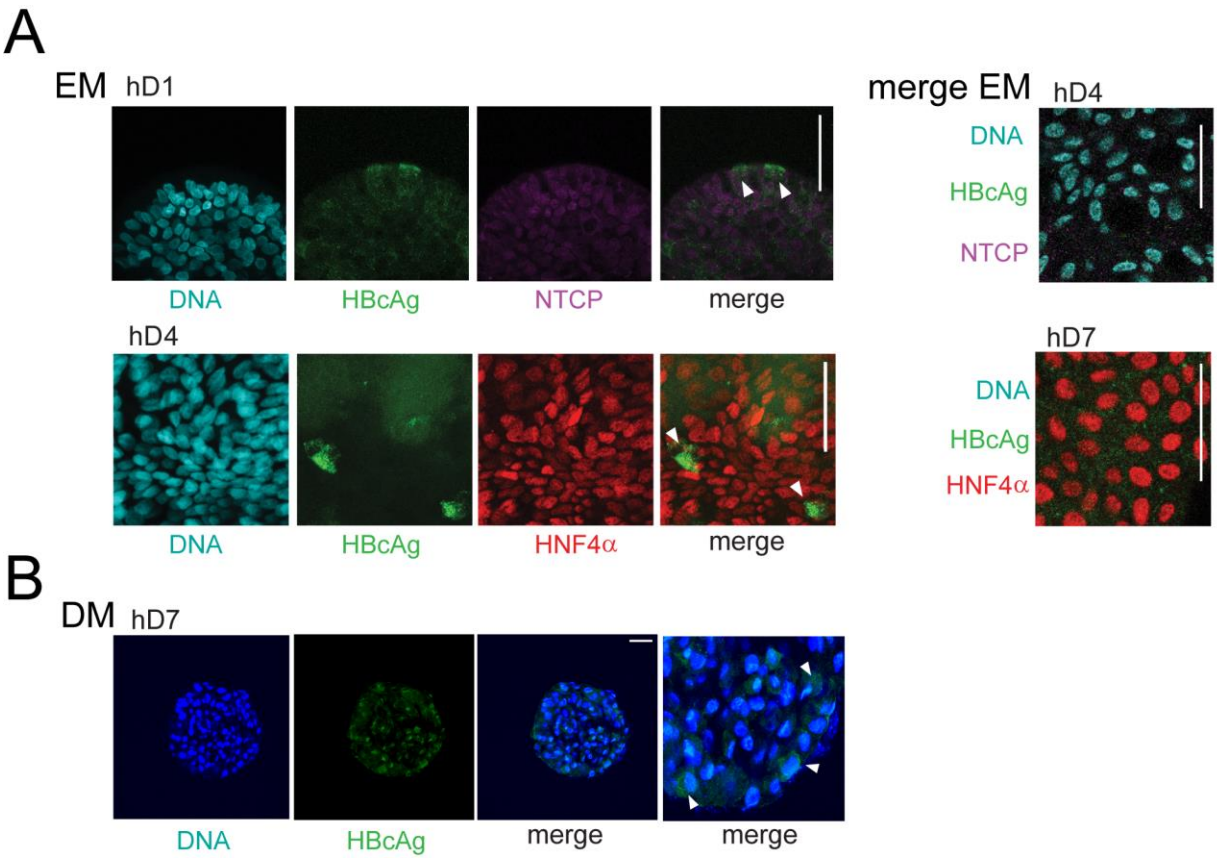

Figure1-figure supplement 1: Expression of HBV core Ag in infected human liver organoids. (A) Immunofluorescent staining showing the expression of HBcAg (green) together with NTCP (magenta) or HNF4α (red) performed in different hD organoids 6 days after HBV infection in expansion condition (EM). (B) Representative immunofleorescent images of differentiated organoid (DM) showing the expression of HBcAg (green) and β-catenin (gray) 6 days after HBV infection.

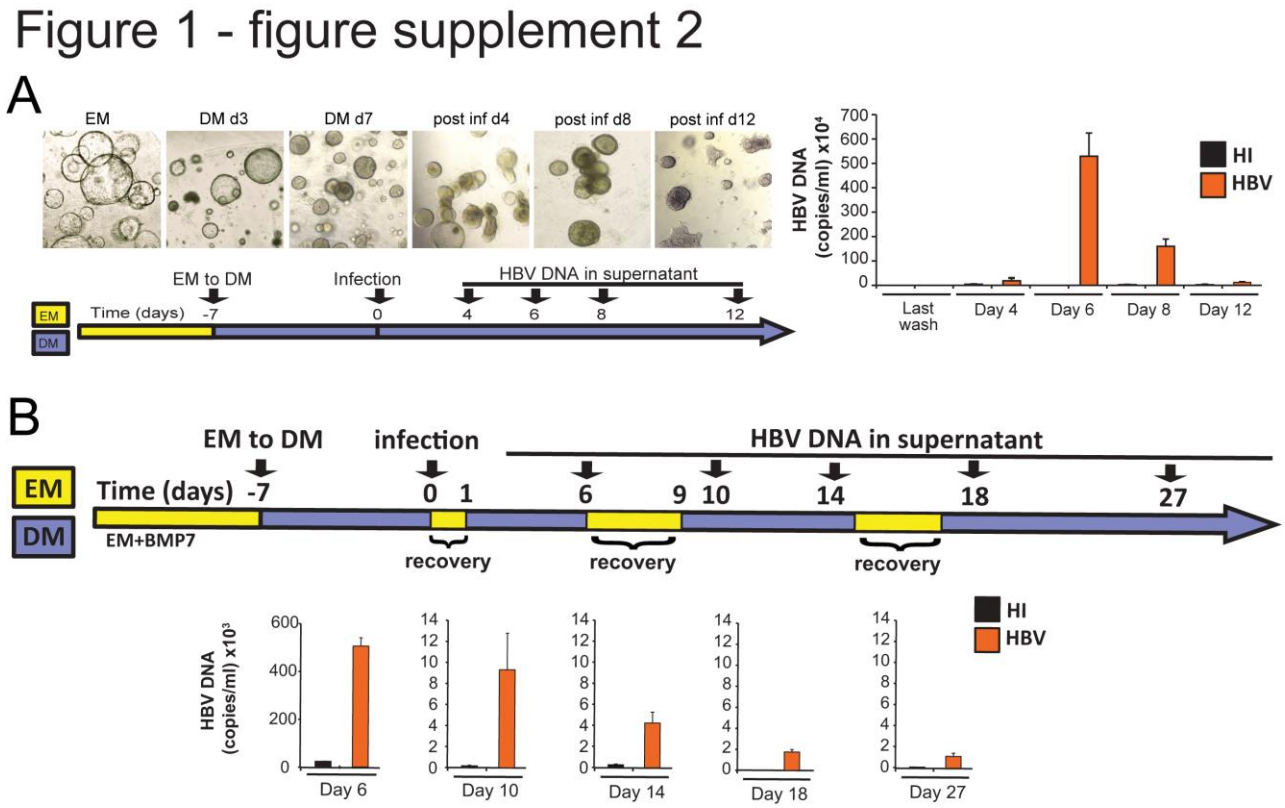

Figure 1 – figure supplement 2: Release of HBV DNA declines over time in hD organoid lines infected in vitro. (A) Bright field images and levels of HBV DNA in the supernatant of infected organoids at different days post infection. (B) HBV DNA in the supernatant of infected organoids undergoing short EM pulse treatments after infection. HBV DNA was quantified by real time PCR and compared to the mock infected (heat inactivated, HI) cultures.

Figure 1 - figure supplement 3

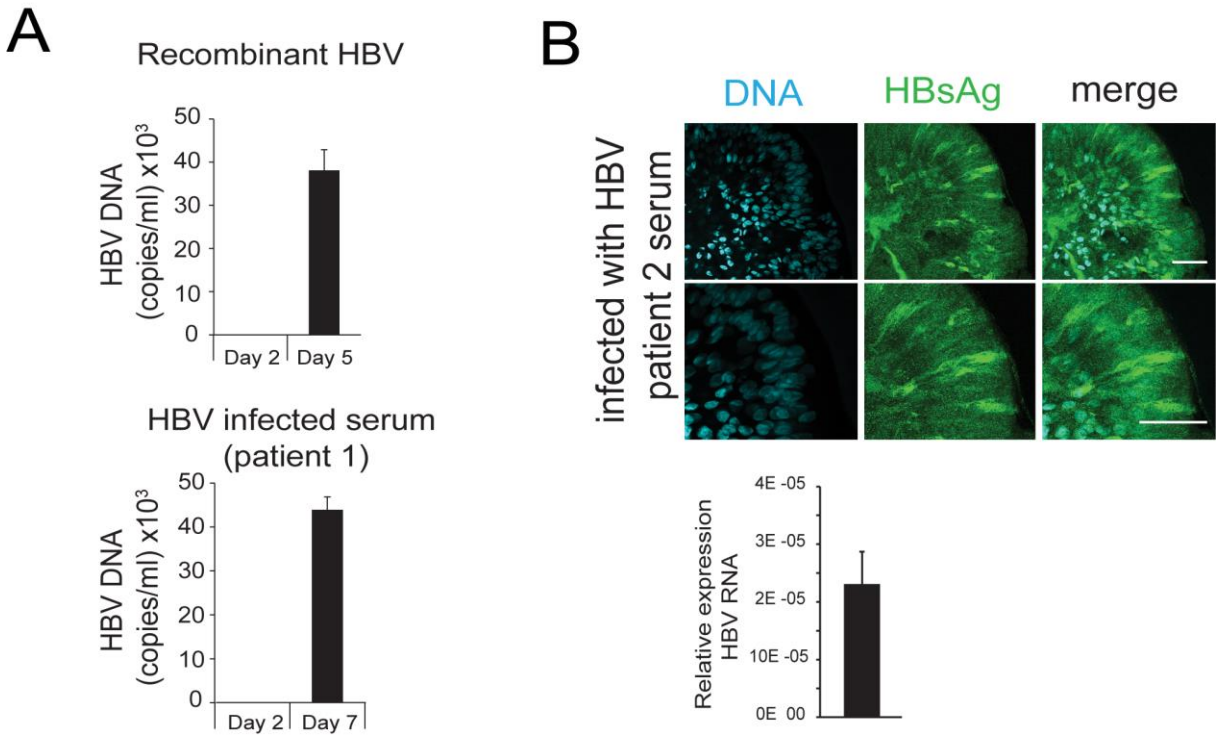

Figure 1 – figure supplement 3: HBV specific DNA, RNA and proteins are detected in hD derived organoids upon infection with recombinant HBV virus as well as with HBV infected patient's serum. (A) Levels of HBV DNA in supernatant of hD organoids infected with either recombinant virus derived from HepG2.2.15 cells or serum obtained from HBV positive individuals (B) Immunofluorescent staining showing the expression of HBV Surface Ag (green) in DM organoids 5 days after infection with serum obtained from HBV positive individuals (patient 2), scale bars represent 50 µm. Bar graph shows total HBV RNA levels in the culture at the time of staining.

Figure 2 - figure supplement 1

A

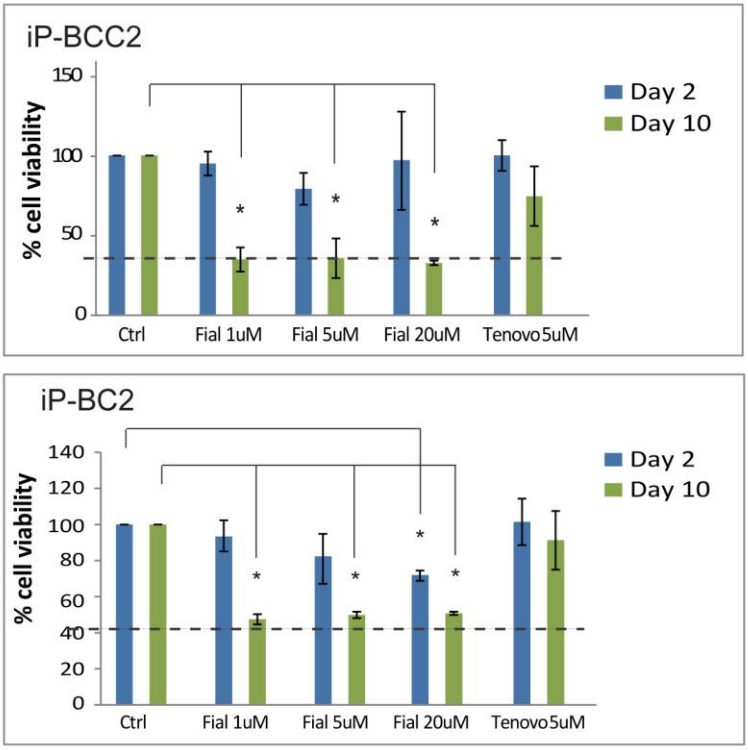

B

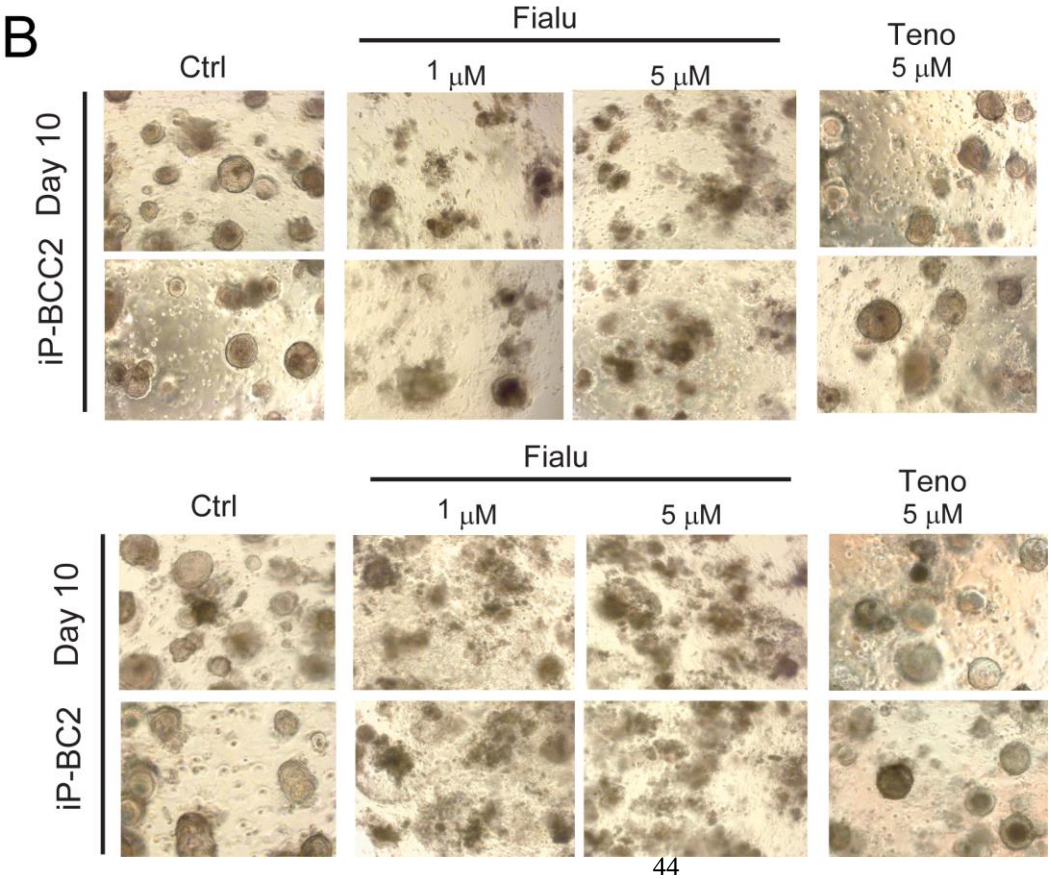

Figure 2 – figure supplement 1: Human liver organoids as a model for anti-HBV drug-induced toxicity screening (A) Bar diagrams representing relative cellular viability of differentiated patient-derived liver organoids (iP-BCC2 and iP-BC2) after 2 or 10 days of treatment with Fialuridine or Tenofovir at the different concentrations indicated using the AlamarBlue cell viability assay. All values are normalized to the vehicle treated control and plotted as the average of percent viability ± SD (n=3). The dotted line represents the lower limit of quantification based on values obtained from wells free of organoids containing the BME matrix only. (B) Representative bright field images taken of differentiated patient-derived liver organoids (iP-BCC2 and iP-BC2) as indicated with Fialuridine and Tenofovir.

Figure 3 - figure supplement 1

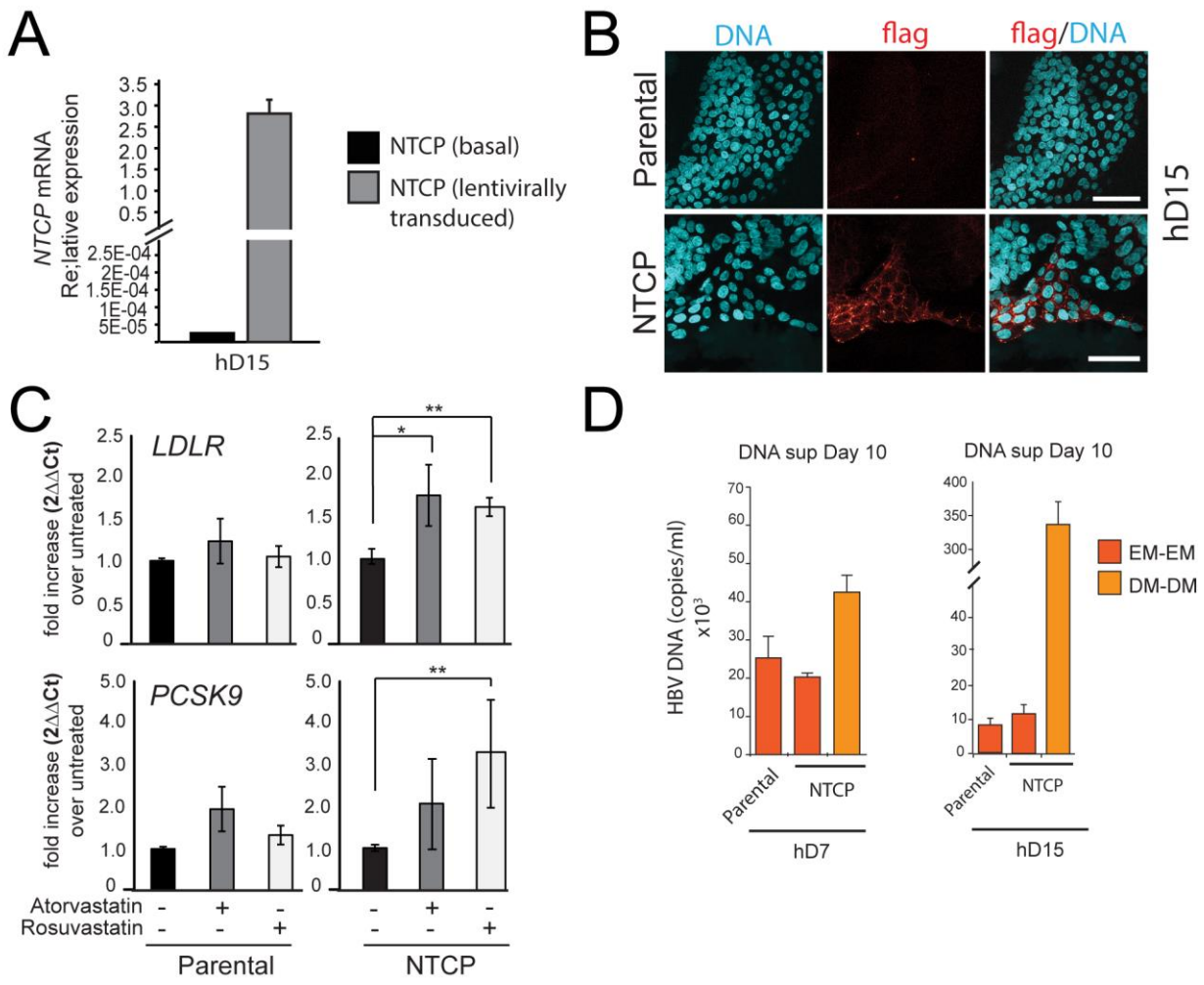

Figure 3 – figure supplement 1: hD organoid lines expressing high levels of functional NTCP can be generated by lentiviral infection. (A) Levels of expression of NTCP were evaluated by RT in the untransduced (Parental) and the transduced (NTCP) lines. Expression of NTCP was calculated according to the 2ΔCt method using the housekeeping gene GAPDH as reference. (B) Expression of NTCP was confirmed by immunofluorescence staining using antibodies against Flag (red). (C) Evaluation of changes in cholesterol metabolism genes following transgenic expression of NTCP in liver organoids. The levels of LDLR and PCSK9 were evaluated by real time PCR following treatment with Atorvastatin and Rosuvastatin. Fold difference in gene expression was calculated according to the 2ΔΔCt method using untreated cells as reference. (D) HBV DNA levels in supernatant of parental cultures grown in EM and NTCP cultures (of donors hD7 and hD15) grown in EM or DM were quantified by real time PCR 10 days after infection.

Figure 3 - figure supplement 2

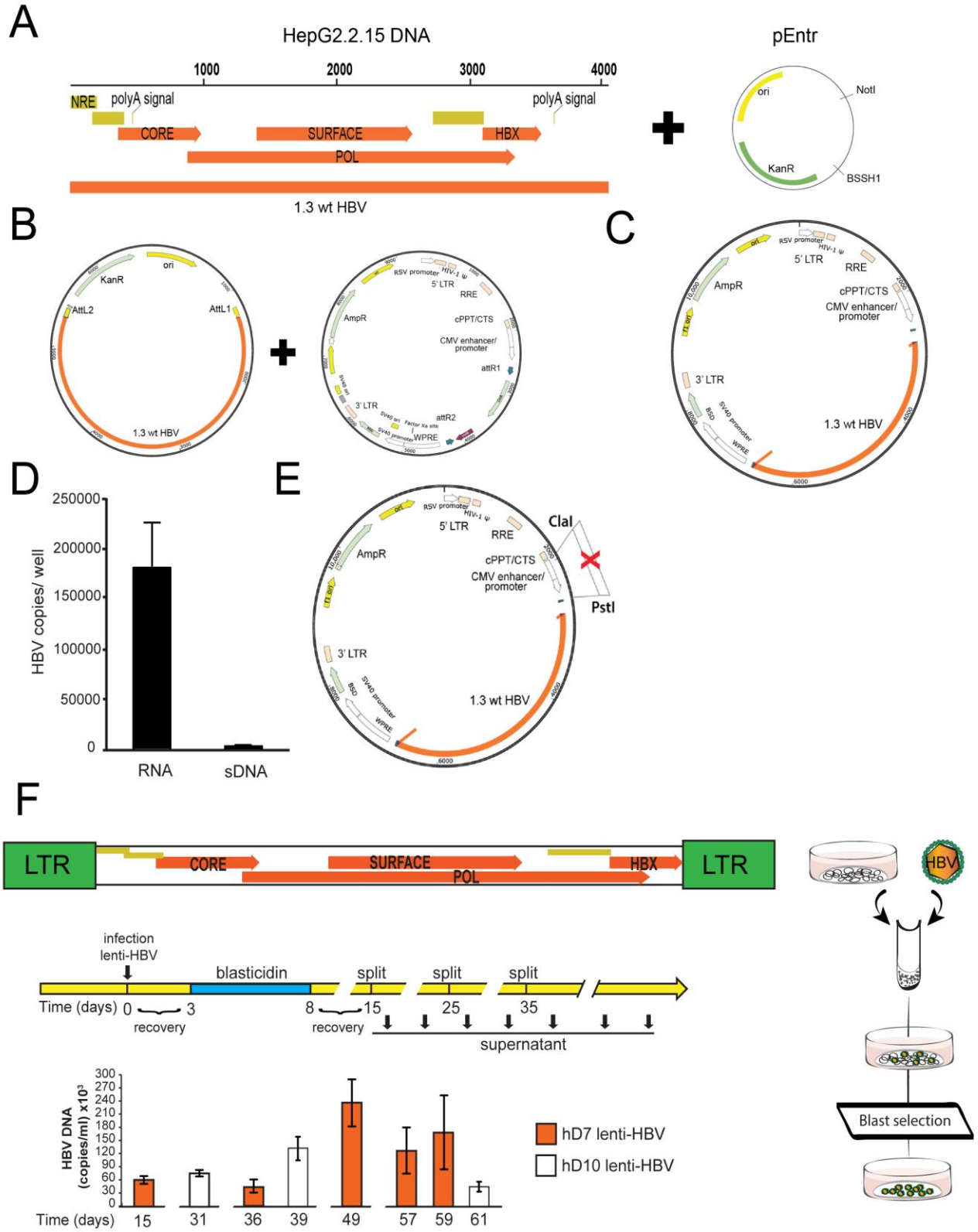

Figure 3 – figure supplement 2: Generation of lentiviral construct used to establish human liver organoid lines expressing viral RNA and releasing virus in the supernatant. (A-B) A fragment encoding 1.3 times the wt HBV genome was amplified from HepG2.2.15 and cloned into the pEntr plasmid. (C) Using the gateway system, HBV was then transferred to a lentiviral expression vector under the control of CMV promoter. (D) Bar charts represent the amount of cellular associated HBV RNA and of HBV DNA released in the supernatant (sDNA) expressed as copies/well of culture. Although HBV RNA could be clearly detected after infection of organoids with the lentiviral construct generated in (B), viral release was minimal, likely because of transcriptional interference due to presence of the strong CMV promoter upstream of HBV genome, which was then removed from the construct (E). (F) Experimental procedure for the generation of transgenic organoid lines expressing full length HBV. EM organoids were infected with a lentiviral vector including a construct encoding 1.3 copies of the HBV genome and selected with blasticidin for 5 days in order to obtain stable transgenic organoid lines. Viral production was determined by real time PCR, measuring the amount of HBV DNA secreted in the supernatant at regular intervals and up to 62 days after lentiviral infection.

Figure 4 - figure supplement 1

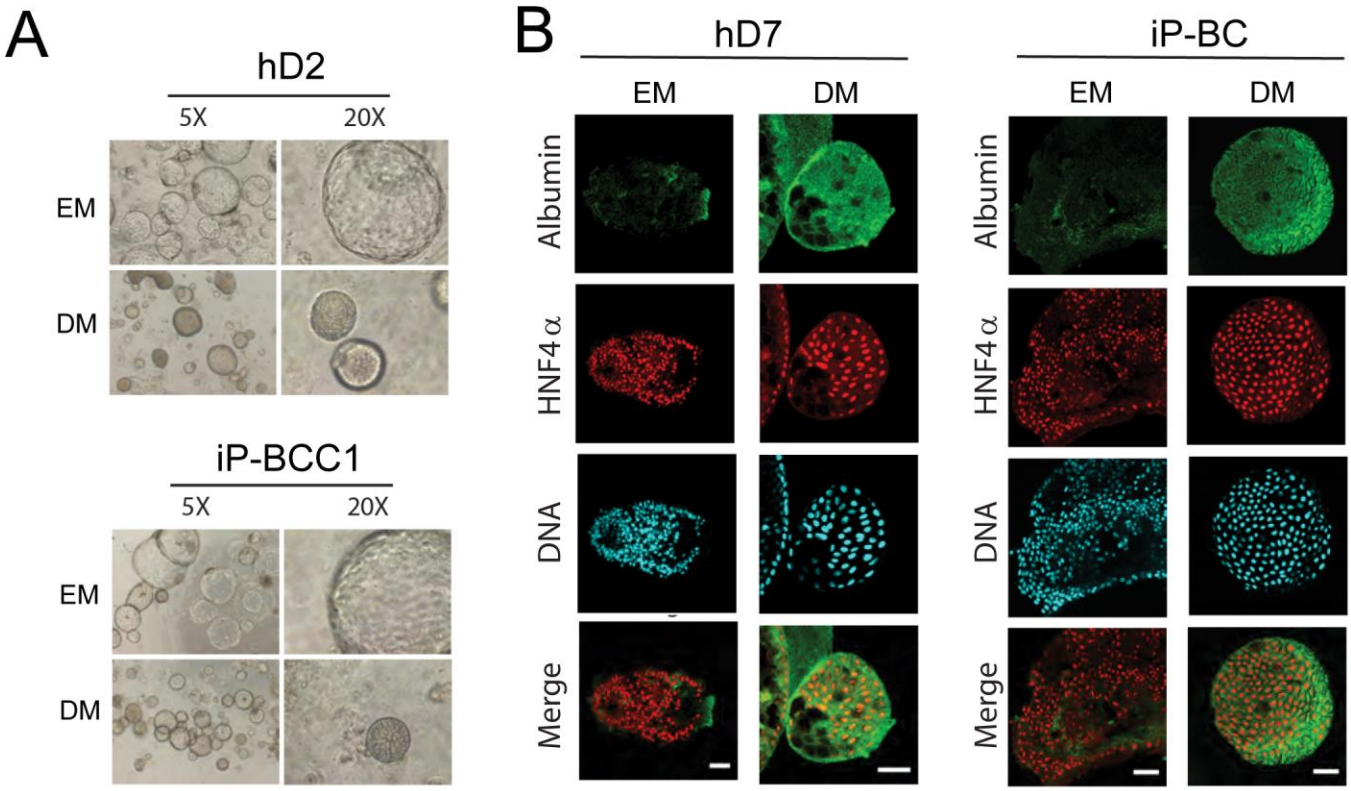

Figure 4 – figure supplement 1: iP derived and hD derived organoids have comparable differentiation potential. (A) Phase contrast images (5X and 20X) magnification of organoid cultures seeded from hDs and iPs show comparable morphological changes in the organization upon differentiation of organoid cultures. (B) Immunofluorescent staining indicates comparable expression of the hepatocyte marker ALB (green) and HNF4α (red) in hD and iP liver organoids in expansion media (EM) and after 7 days of culture in differentiation media (DM). Nuclei are counterstained with Hoechst 33342 (cyan). Scale bars represent 50 µm.

Table S1. Characteristics of patients included in the study

Patients	**Age**	**Sex**	**Diagnosis**	Treatment (Y/N)	HBsAg (P/N)	HBcAg (P/N)	HBeAg (P/N)	anti HBsAg	anti HBcAg	anti HBeAg	DNA
iD	44	F	DONOR, cleared HBV	N	N	NA	NA	P	P	NA	NA
iP-BC	49	M	Liver cirrhosis based on chronic HBV infection and portal hypertension	Y	P	NA	NA	P	P	NA	<20
iP-BCC	65	M	HBV liver cirrhosis with HCC	Y	P	NA	NA	N	P	NA	NA
iP-BCC2	54	M	Chronic liver cirrhosis along with HCC	Y	P	NA	NA	N	P	NA	<20
iP-BCC3	68	M	Chronic HBV liver cirrhosis with HCC, vital tumor at the moment of transplantation	Y	P	NA	NA	N	P	NA	<20
iP-BCC4	52	M	HBV liver cirrhosis with multiple HCC	Y	P	NA	N	N	P	P	<20
iP-BFA	54	F	Acute liver failure with Crohn's disease	N	P	NA	N	N	P	P	<20
iP-BFA2	62	M	Acute liver failure based on HBV	N	P	NA	NA	P	P	NA	NA
iP-BDFA	28	M	Acute liver failure based on HBV and co-infected with HDV	N	P	NA	N	NA	P	P	1180
iP-B	60	F	Acute or chronic liver failure based on HBV infection	Y	P	NA	NA	N	P	NA	1080
iP-BDCC	59	M	HCC, HBV co-infected with HDV	Y	P	NA	NA	N	P	P	<20

Table S2. Gene expression signature

	log2 of DESeq normalized counts									
gene_name	hD1	hD7	hD8	hD9	hD10	iP2	iP3	iP5	iP6	iP7
SPC24	5,78136	6,06609	6,50779	6,14975	6,24793	4,52356	6,00000	4,52356	4,70044	5,20945
TMEM38A	5,58496	7,10852	5,83289	6,30378	6,33985	4,16993	5,32193	4,24793	4,85798	4,75489
TMEM229B	4,58496	5,78136	5,83289	5,70044	6,49185	5,55459	5,39232	3,90689	4,16993	3,70044
SLC39A5	5,04439	5,24793	6,80735	6,42626	6,06609	4,08746	5,32193	3,00000	3,58496	5,12928
PDE4C	4,70044	5,72792	6,91886	5,04439	6,98868	4,39232	3,90689	3,90689	3,16993	5,52356
COLCA2	4,24793	6,89482	6,04439	4,58496	7,05528	3,00000	5,12928	4,08746	4,24793	3,80735
ME1	4,32193	6,04439	4,90689	5,16993	7,12928	4,16993	4,32193	2,80735	4,32193	4,70044
HHAT	5,64386	5,55459	5,45943	4,80735	4,58496	3,90689	5,20945	4,16993	3,00000	4,08746
UAP1L1	5,32193	5,24793	5,39232	4,58496	5,80735	3,45943	4,58496	4,08746	3,00000	4,08746
RAB6B	5,75489	5,42626	5,67243	4,52356	5,42626	4,75489	3,58496	4,08746	3,16993	4,08746
BHLHE41	5,42626	6,06609	5,78136	4,90689	5,93074	4,32193	4,70044	3,58496	4,70044	4,32193
KLHL17	4,75489	5,35755	5,88264	5,08746	5,00000	3,45943	3,80735	4,39232	4,85798	4,08746
NBPF3	6,32193	6,12928	5,78136	3,58496	6,47573	4,00000	4,39232	3,90689	3,58496	4,24793
C2CD4B	4,75489	5,45943	6,56986	3,80735	6,06609	3,00000	4,70044	4,00000	3,58496	4,08746
CTC1	6,18982	5,35755	5,24793	6,52356	5,70044	5,04439	5,32193	4,85798	3,58496	4,80735
C15orf38	5,42626	5,64386	5,45943	5,58496	6,08746	5,32193	5,04439	4,52356	3,00000	4,32193
CDHR5	5,67243	6,20945	6,47573	6,30378	5,97728	4,45943	4,70044	5,72792	2,80735	5,24793
ECM1	4,75489	6,44294	5,32193	5,20945	5,80735	4,08746	4,80735	4,90689	3,58496	4,45943
NBPF14	4,85798	5,12928	5,28540	6,28540	5,32193	3,32193	4,85798	4,75489	3,70044	4,70044
SYT17	5,78136	5,88264	6,40939	5,52356	5,49185	3,00000	5,42626	5,16993	4,52356	4,16993
CHST11	6,16993	5,20945	5,00000	5,67243	5,61471	3,45943	3,90689	3,80735	4,24793	4,52356
DHRS13	5,97728	4,70044	4,80735	6,39232	5,95420	2,32193	3,80735	4,58496	3,70044	5,16993
DIAPH2	6,06609	5,75489	4,08746	5,52356	5,88264	2,58496	5,28540	4,32193	3,45943	4,85798
ZNF488	6,20945	4,08746	6,53916	6,12928	5,78136	2,58496	4,95420	3,70044	2,80735	5,32193
PDZD3	6,06609	7,03342	6,53916	6,53916	6,75489	1,00000	6,28540	3,00000	5,58496	4,95420
MECOM	5,83289	6,71425	5,08746	6,40939	5,61471	1,58496	5,12928	4,39232	5,49185	3,58496
CLRN3	6,20945	5,61471	5,88264	5,88264	7,51570	1,00000	5,39232	4,64386	4,32193	6,59991
CA2	5,16993	6,93074	6,40939	6,26679	7,43463	1,58496	4,52356	3,58496	3,45943	5,00000
SPP1	6,04439	6,04439	5,70044	7,62205	6,40939	4,16993	4,70044	5,78136	6,42626	4,45943
PIGB	6,35755	5,52356	4,64386	8,24793	5,83289	3,00000	5,83289	5,16993	5,83289	4,58496
RP11-159D12.5	6,84549	7,30378	4,80735	6,33985	6,53916	3,45943	5,12928	5,55459	5,35755	5,16993
ELFN2	6,90689	6,83289	7,34873	6,75489	6,91886	5,12928	5,45943	4,70044	5,32193	5,42626
TTC39A	6,75489	6,22882	6,91886	5,70044	6,20945	5,78136	5,45943	5,20945	5,08746	5,00000
PIDD	5,88264	6,74147	7,53138	6,83289	6,00000	5,12928	4,64386	5,93074	5,78136	5,08746
GPRIN2	5,95420	5,58496	7,65105	6,39232	5,58496	5,49185	5,75489	5,20945	4,24793	5,72792
CCDC24	5,39232	5,52356	6,94251	8,01123	5,58496	5,08746	5,49185	5,52356	5,20945	4,80735
SLC6A20	5,45943	7,00000	8,34430	6,18982	7,28540	3,45943	5,88264	6,02237	5,04439	5,70044
DACT2	4,95420	6,97728	7,55459	5,97728	7,03342	5,61471	6,37504	5,88264	4,95420	2,58496
ZBED3	5,88264	6,88264	6,33985	4,24793	6,56986	4,80735	4,90689	5,58496	4,90689	4,08746
EHD2	5,20945	6,96578	5,90689	5,49185	6,02237	4,00000	3,16993	5,61471	3,70044	3,00000
WNK2	5,67243	6,62936	7,27612	5,80735	6,04439	4,64386	4,95420	4,39232	4,70044	2,58496
EVC	5,58496	6,06609	5,28540	5,78136	6,02237	3,58496	5,45943	5,04439	4,90689	2,32193
NAGPA	5,88264	5,61471	6,16993	7,01123	7,14975	5,20945	5,61471	5,67243	4,95420	5,04439
CYP2C18	6,28540	5,70044	6,24793	6,62936	6,88264	5,20945	5,24793	4,85798	4,24793	5,45943
TMEM86B	5,88264	5,78136	6,53916	6,12928	7,37504	5,08746	6,04439	5,78136	3,45943	4,95420
DHRS11	6,00000	6,74147	7,05528	7,40939	6,35755	5,20945	6,22882	6,00000	3,16993	6,32193
ZXDC	6,56986	6,52356	5,72792	6,91886	6,47573	5,42626	5,97728	6,35755	3,16993	4,45943
SLC12A8	5,61471	6,39232	6,30378	7,09803	5,72792	4,64386	5,24793	5,39232	5,39232	5,24793
LYPD6	6,16993	5,85798	6,30378	6,67243	5,32193	4,24793	4,70044	5,20945	4,70044	5,39232
RMI2	6,44294	6,37504	5,95420	7,49185	6,47573	5,08746	4,52356	5,28540	5,08746	6,59991
HMHA1	6,79442	6,02237	5,72792	6,82018	4,90689	4,08746	5,49185	4,80735	3,58496	5,95420
KRT13	7,30378	5,70044	8,87036	6,61471	6,84549	4,58496	4,70044	6,22882	3,45943	7,66534
AIFM2	7,53138	6,49185	7,74819	6,37504	6,37504	4,00000	5,24793	6,00000	2,80735	6,72792
AKR1C2	4,70044	7,69349	6,79442	8,20457	8,66534	3,90689	7,45121	7,03342	2,80735	5,95420
SLC16A1	7,40088	8,19476	7,62936	7,33092	8,26209	4,39232	5,42626	5,08746	5,88264	7,04439
NOSTRIN	7,13955	8,30378	6,08746	6,84549	7,24793	3,58496	6,50779	5,39232	6,12928	6,02237
MUC17	8,21917	6,62936	6,20945	6,33985	8,11894	3,45943	6,71425	4,85798	4,45943	6,94251
KIF13A	7,39232	6,37504	6,55459	7,31288	6,39232	4,08746	6,32193	6,08746	4,85798	6,40939
TNNI2	7,19967	7,74147	8,04439	6,28540	5,78136	3,80735	6,70044	3,16993	6,59991	4,45943
CALB2	6,75489	8,14975	6,85798	5,90689	7,33092	4,90689	5,49185	2,32193	4,75489	6,35755

FABP1	10,04712	6,35755	6,28540	9,19229	6,47573	3,45943	5,04439	1,58496	4,90689	6,18982
LYPD6B	5,80735	5,45943	5,67243	5,72792	4,80735	3,00000	4,70044	4,52356	3,70044	2,80735
PASK	4,95420	4,85798	4,75489	5,35755	5,04439	2,58496	4,24793	4,45943	3,00000	3,32193
GLMN	5,85798	4,70044	4,64386	6,22882	4,58496	3,45943	4,52356	3,32193	4,00000	2,32193
BTNL9	5,58496	4,45943	6,84549	6,62936	2,80735	2,32193	5,32193	4,39232	2,32193	2,32193
PF4	5,16993	5,90689	5,67243	7,93664	6,00000	1,58496	5,55459	2,80735	2,80735	2,00000
DKK3	5,97728	6,35755	7,51570	6,18982	3,45943	2,32193	5,12928	3,45943	4,90689	3,70044
SPRR1A	7,70044	2,32193	6,00000	6,26679	4,90689	0,00000	3,90689	5,58496	2,32193	3,45943
GYG2	5,52356	5,52356	5,88264	5,64386	4,58496	0,00000	6,40939	2,58496	0,00000	3,90689
SLC17A9	6,06609	6,10852	5,67243	6,04439	6,78136	3,70044	5,08746	3,90689	0,00000	5,45943
MYZAP	5,12928	5,28540	4,80735	5,45943	5,97728	3,00000	4,00000	4,32193	1,00000	4,95420
MX1	4,70044	4,24793	6,02237	7,12928	5,55459	5,55459	5,12928	4,00000	0,00000	3,00000
APBB1IP	5,64386	4,32193	5,24793	7,32193	4,64386	4,95420	4,85798	3,32193	0,00000	4,80735
PPBP	6,04439	4,85798	5,70044	9,48382	2,00000	4,85798	4,64386	5,85798	0,00000	4,39232
IFI27	5,32193	8,70736	4,24793	8,11894	11,98335	4,39232	3,58496	3,58496	5,24793	2,32193
CLDN18	3,58496	7,99435	5,70044	4,00000	9,51964	5,20945	4,39232	7,39232	5,24793	0,00000
ANKRD50	5,28540	5,24793	4,80735	4,24793	4,16993	6,42626	5,80735	5,04439	6,53916	5,52356
PKIG	4,90689	5,00000	4,70044	3,58496	4,70044	6,45943	5,80735	5,16993	6,14975	5,28540
SH3BP5	4,32193	4,70044	4,75489	4,24793	3,58496	6,24793	5,45943	4,58496	6,26679	5,35755
ACAP1	4,08746	5,12928	5,16993	3,32193	4,52356	6,42626	6,84549	5,58496	4,90689	4,90689
RNF144B	4,08746	4,16993	5,12928	2,00000	5,52356	5,83289	5,24793	5,70044	5,97728	5,72792
ST6GAL2	4,52356	4,08746	4,45943	5,52356	4,64386	5,90689	5,42626	6,83289	6,53916	4,75489
ZNF551	3,70044	4,45943	4,08746	4,75489	4,45943	5,72792	5,24793	5,55459	5,67243	5,04439
ATF3	2,58496	4,90689	3,70044	2,58496	5,42626	4,70044	5,83289	7,58496	6,30378	4,00000
FGA	2,58496	3,80735	5,08746	4,00000	3,00000	4,24793	5,85798	6,71425	5,90689	3,00000
GZF1	4,32193	3,58496	2,58496	4,39232	3,70044	4,39232	4,95420	5,28540	6,49185	4,95420
SESN3	5,35755	4,08746	2,58496	3,45943	2,00000	5,67243	4,32193	4,64386	7,45943	4,08746
EVA1B	4,16993	3,45943	3,32193	3,80735	3,16993	7,11894	3,90689	4,45943	5,83289	5,42626
CD14	2,32193	3,90689	3,80735	4,45943	2,58496	4,70044	4,08746	4,16993	7,20945	4,45943
RAPGEF3	4,08746	3,00000	4,80735	2,58496	3,45943	5,64386	5,39232	5,55459	5,35755	3,45943
PTHLH	3,58496	2,32193	4,08746	2,00000	2,32193	5,58496	5,45943	4,64386	4,52356	4,39232
ADAMTS1	3,45943	2,80735	3,90689	4,16993	3,00000	5,49185	6,96578	5,28540	4,70044	3,32193
UGT2B11	4,16993	1,58496	2,58496	6,08746	4,52356	2,58496	6,52356	6,64386	6,87036	6,70044
UGT2B7	3,80735	4,32193	4,45943	5,45943	6,33985	5,95420	5,45943	6,45943	6,52356	6,90689
FRG1B	4,32193	5,16993	3,00000	4,52356	5,64386	6,30378	5,80735	5,64386	6,06609	6,08746
CENPC	4,58496	5,04439	3,00000	5,35755	5,55459	6,47573	4,80735	5,12928	5,52356	8,19476
COPG2	4,16993	5,32193	3,32193	3,32193	5,04439	7,15987	4,52356	4,95420	4,45943	6,58496
BEX5	3,32193	4,24793	3,80735	2,80735	5,39232	7,54689	2,58496	6,75489	5,49185	6,06609
IFT52	4,90689	5,45943	5,58496	5,61471	4,70044	6,64386	5,80735	5,80735	6,75489	6,44294
PEX11G	4,70044	4,70044	5,67243	5,08746	5,49185	6,87036	5,95420	5,42626	6,45943	6,14975
PLEKHG5	5,55459	5,35755	4,90689	5,20945	6,12928	7,66534	6,00000	5,88264	6,06609	7,24793
C4orf48	5,90689	3,90689	5,78136	5,70044	3,80735	8,25739	4,39232	6,28540	7,01123	6,74147
NEDD8-MDP1	6,80735	7,05528	6,28540	6,42626	6,58496	7,78136	7,97154	7,20945	8,88264	6,74147
CASP4	6,79442	6,62936	6,53916	5,83289	6,83289	7,98868	7,67243	7,44294	7,94837	6,82018
GABBR1	6,68650	6,12928	6,26679	6,45943	6,12928	8,59619	7,82018	6,67243	7,78136	6,24793
MDP1	6,20945	6,47573	5,49185	5,80735	5,97728	7,16993	7,37504	6,64386	8,27146	5,93074
PFDN4	6,67243	6,24793	6,18982	6,45943	6,14975	7,98299	6,62936	6,91886	7,83289	7,54689
MED21	6,52356	6,79442	5,24793	6,89482	6,47573	6,20945	7,72792	7,10852	8,23362	7,65105
MAPK11	5,95420	5,85798	6,04439	5,90689	4,58496	8,08746	5,95420	7,26679	7,68650	6,74147
PTK7	4,85798	5,97728	5,83289	5,49185	4,08746	8,40939	6,78136	7,12928	6,40939	6,26679
LRG1	6,10852	6,08746	6,72792	4,70044	4,85798	6,89482	6,90689	6,82018	7,83289	5,72792
PTGES	7,51570	5,85798	6,35755	6,50779	5,20945	9,72451	7,74819	7,26679	7,20945	7,15987
HLA-DMA	6,30378	3,90689	7,12928	2,80735	6,78136	8,40939	7,63662	7,03342	7,48382	4,45943
CST6	5,83289	4,52356	3,80735	5,28540	3,90689	8,55459	6,14975	5,32193	7,53138	4,39232
UBD	5,24793	3,58496	4,90689	4,32193	3,16993	8,40514	7,09803	2,80735	7,12928	4,58496
EFEMP1	6,62936	5,08746	3,32193	3,58496	2,00000	7,12928	6,72792	5,64386	6,30378	6,39232
MFAP5	7,68650	1,00000	1,00000	5,52356	4,90689	9,77643	7,36632	5,35755	6,65821	6,90689
ZNF765	5,16993	4,85798	4,52356	4,52356	4,58496	1,00000	3,80735	4,00000	4,58496	2,80735
CREG2	4,39232	4,32193	3,90689	4,52356	5,04439	1,58496	3,45943	3,80735	3,90689	2,32193
SLC9A4	4,80735	5,12928	4,52356	4,32193	4,85798	0,00000	2,58496	2,80735	4,52356	3,00000
PSAPL1	4,75489	4,75489	5,08746	5,72792	6,49185	0,00000	3,16993	4,08746	3,90689	2,32193
UVSSA	4,58496	5,70044	5,83289	5,04439	4,90689	1,58496	4,58496	5,04439	2,32193	0,00000
TLR6	4,39232	5,00000	3,45943	4,95420	5,85798	0,00000	3,16993	4,00000	2,32193	0,00000

TMEM231	4,52356	4,45943	4,45943	4,52356	4,00000	3,45943	2,58496	2,00000	3,16993	3,00000
GRK4	4,90689	4,64386	4,52356	4,24793	2,00000	4,08746	2,32193	2,58496	2,32193	2,00000
IRAK2	4,39232	4,52356	3,90689	5,35755	4,58496	4,90689	3,16993	3,16993	2,00000	1,58496
BPIFB1	5,00000	4,08746	5,93074	4,52356	3,70044	3,80735	3,32193	3,16993	4,32193	0,00000
SEC16B	4,70044	5,55459	4,45943	2,80735	3,16993	2,32193	4,08746	2,32193	3,00000	1,00000
RUSC2	4,24793	4,08746	3,90689	3,58496	3,90689	2,58496	2,32193	3,00000	1,00000	0,00000
AGAP5	4,00000	4,95420	4,64386	4,90689	3,58496	2,32193	4,08746	3,58496	2,00000	3,00000
AGMO	4,32193	4,32193	4,95420	4,39232	4,85798	0,00000	3,80735	3,32193	1,00000	3,32193
SLC35F3	5,39232	5,39232	4,90689	3,45943	3,32193	1,58496	4,58496	3,58496	0,00000	3,16993
SIMC1	3,80735	4,08746	5,00000	2,58496	4,95420	3,32193	2,58496	2,80735	1,00000	2,80735
CIDEC	3,32193	3,80735	5,08746	4,00000	4,32193	2,32193	2,00000	1,58496	0,00000	2,58496
TNFRSF1B	4,64386	5,49185	5,08746	4,90689	6,49185	3,58496	4,52356	2,32193	1,00000	2,80735
MOGAT3	4,39232	4,75489	4,90689	4,85798	5,20945	2,00000	4,32193	2,32193	0,00000	3,90689
CYP4F2	2,58496	6,10852	5,00000	3,32193	7,33092	3,00000	4,85798	2,80735	0,00000	3,32193
ANK1	3,32193	6,20945	6,74147	4,45943	5,83289	3,45943	5,12928	4,58496	0,00000	0,00000
PDZK1	4,39232	3,80735	3,90689	4,52356	1,58496	0,00000	3,45943	1,58496	0,00000	2,58496
SHANK3	2,80735	3,00000	3,80735	4,85798	2,58496	0,00000	2,58496	2,00000	0,00000	3,00000
TMEM27	4,58496	3,80735	3,00000	4,45943	2,80735	1,00000	3,58496	1,58496	0,00000	1,00000
ADRA2C	2,80735	4,39232	4,90689	4,08746	2,00000	1,00000	3,80735	0,00000	1,00000	2,32193
C2CD4A	3,32193	4,32193	6,24793	4,52356	3,58496	1,00000	2,80735	3,00000	0,00000	2,32193
RNF157	2,00000	4,75489	4,39232	4,45943	3,00000	1,00000	3,45943	2,58496	1,00000	2,00000
SOWAHD	1,58496	2,80735	4,45943	3,00000	4,00000	0,00000	2,58496	1,58496	0,00000	1,58496
KCNH3	2,58496	1,00000	4,90689	4,90689	4,80735	3,00000	3,16993	0,00000	0,00000	2,32193
USPL1	2,80735	3,32193	2,32193	4,90689	6,12928	1,58496	3,16993	3,45943	1,00000	2,58496
EPSTI1	4,16993	3,00000	1,00000	6,26679	4,24793	1,58496	3,32193	1,58496	2,32193	1,00000
PINLYP	3,58496	4,70044	4,64386	2,00000	2,00000	1,00000	2,00000	2,80735	2,32193	0,00000
SLC13A3	3,90689	3,45943	5,39232	2,00000	1,00000	0,00000	2,00000	2,80735	2,32193	0,00000
FOXD2	3,70044	4,39232	4,70044	3,45943	3,32193	0,00000	2,58496	4,00000	2,32193	0,00000
IL1RL1	2,32193	4,64386	4,16993	3,00000	4,58496	0,00000	1,00000	2,00000	3,70044	0,00000
GSTA1	2,00000	2,58496	5,12928	3,45943	4,58496	0,00000	1,00000	2,00000	3,00000	0,00000
METTL21B	2,00000	5,35755	4,08746	3,45943	3,45943	1,00000	2,80735	1,00000	2,00000	0,00000
SLC14A1	0,00000	4,80735	3,45943	3,45943	3,16993	1,58496	1,00000	2,32193	1,00000	0,00000
ODAM	1,00000	5,49185	3,90689	0,00000	3,45943	0,00000	2,32193	1,58496	1,00000	0,00000
DNHD1	4,08746	5,32193	4,70044	2,32193	4,80735	0,00000	4,08746	4,64386	0,00000	0,00000
SULT1B1	2,80735	5,00000	3,16993	1,00000	6,12928	0,00000	3,80735	2,32193	0,00000	1,00000
TMEM213	3,00000	7,79442	4,45943	1,58496	2,00000	0,00000	1,00000	4,45943	0,00000	1,00000
SULT1C2	2,58496	5,24793	0,00000	3,90689	7,32193	0,00000	1,00000	1,00000	0,00000	1,00000
GKN1	2,00000	6,90689	0,00000	0,00000	6,71425	0,00000	0,00000	1,00000	0,00000	0,00000
CCNB3	4,00000	4,52356	0,00000	1,58496	4,90689	2,00000	2,00000	0,00000	0,00000	0,00000
PGC	6,37504	5,16993	3,00000	0,00000	7,38370	4,70044	2,58496	0,00000	0,00000	3,45943
RGN	2,58496	1,58496	3,32193	2,00000	1,58496	1,00000	1,00000	1,00000	0,00000	0,00000
TUBA8	2,80735	2,00000	2,32193	2,32193	1,58496	0,00000	1,00000	1,00000	0,00000	0,00000
CYP3A4	2,58496	2,00000	3,32193	1,58496	2,32193	0,00000	1,00000	1,00000	1,00000	1,00000
C7orf31	3,45943	2,58496	2,32193	1,58496	2,32193	1,58496	0,00000	1,58496	0,00000	0,00000
CTD-3193O13.9	3,00000	1,58496	3,16993	1,58496	2,00000	1,00000	0,00000	0,00000	0,00000	0,00000
CA14	3,45943	3,70044	3,32193	2,00000	2,58496	0,00000	0,00000	1,58496	0,00000	0,00000
ACRC	2,80735	3,70044	2,58496	2,80735	1,00000	0,00000	0,00000	1,00000	0,00000	0,00000
NR1H4	2,32193	1,00000	2,58496	2,80735	2,58496	0,00000	0,00000	0,00000	0,00000	1,00000
USP18	2,32193	0,00000	2,58496	3,58496	2,58496	1,00000	0,00000	0,00000	0,00000	0,00000
VWCE	1,00000	1,00000	4,08746	1,58496	3,32193	1,00000	0,00000	0,00000	0,00000	0,00000
C12orf60	2,58496	2,58496	0,00000	3,00000	3,90689	0,00000	0,00000	1,00000	0,00000	0,00000
DNAH12	1,58496	3,00000	0,00000	2,58496	3,45943	0,00000	0,00000	0,00000	0,00000	0,00000
ZNF239	1,58496	2,80735	1,00000	2,00000	4,08746	0,00000	1,00000	0,00000	1,00000	0,00000
CYP2C19	2,58496	1,00000	0,00000	2,32193	4,16993	0,00000	0,00000	1,00000	0,00000	0,00000
FHAD1	1,00000	1,00000	0,00000	2,80735	4,00000	0,00000	0,00000	1,00000	0,00000	0,00000
TIMP4	2,00000	2,32193	1,00000	2,58496	4,39232	0,00000	0,00000	1,58496	0,00000	1,00000
C11orf86	2,80735	2,32193	0,00000	0,00000	3,45943	0,00000	0,00000	0,00000	0,00000	0,00000
RAET1G	2,58496	2,00000	0,00000	0,00000	3,58496	0,00000	0,00000	0,00000	0,00000	0,00000
GCK	2,80735	1,58496	0,00000	0,00000	3,00000	0,00000	0,00000	0,00000	0,00000	0,00000
RASSF9	2,58496	2,32193	1,00000	1,00000	2,00000	0,00000	0,00000	1,00000	0,00000	0,00000
PGF	1,58496	2,32193	3,16993	1,00000	1,58496	0,00000	0,00000	1,00000	0,00000	0,00000
SYNC	1,00000	2,00000	3,00000	1,00000	2,00000	0,00000	0,00000	1,00000	0,00000	0,00000
KCNQ4	1,58496	2,80735	3,00000	0,00000	1,58496	0,00000	0,00000	1,00000	0,00000	0,00000

C1orf177	1,58496	2,32193	2,58496	0,00000	3,00000	0,00000	0,00000	0,00000	0,00000	0,00000
RPS6KA6	2,80735	3,32193	3,32193	0,00000	2,00000	0,00000	0,00000	1,58496	0,00000	0,00000
TCTE1	1,58496	2,80735	3,32193	2,58496	3,00000	0,00000	0,00000	2,58496	0,00000	0,00000
LNP1	1,00000	3,00000	3,00000	2,32193	3,45943	0,00000	0,00000	2,00000	0,00000	0,00000
KCNH8	1,00000	3,32193	4,80735	0,00000	4,16993	0,00000	0,00000	1,58496	0,00000	0,00000
PRSS21	0,00000	0,00000	6,44294	1,00000	2,32193	0,00000	0,00000	1,00000	0,00000	0,00000
SALL1	3,90689	2,32193	3,16993	0,00000	0,00000	0,00000	0,00000	0,00000	0,00000	0,00000
GRIN3B	2,32193	3,00000	3,16993	0,00000	0,00000	0,00000	0,00000	0,00000	0,00000	0,00000
KCNN1	2,32193	1,00000	3,32193	0,00000	1,00000	0,00000	0,00000	0,00000	0,00000	0,00000
KCNS1	1,58496	0,00000	3,90689	1,58496	0,00000	0,00000	0,00000	0,00000	0,00000	0,00000
GATA5	3,32193	3,70044	4,90689	3,70044	2,00000	3,70044	0,00000	1,00000	1,00000	2,00000
CDHR3	2,80735	2,80735	3,70044	3,00000	2,00000	2,32193	0,00000	1,58496	1,00000	1,00000
SLC11A1	2,58496	4,08746	3,90689	3,00000	3,58496	3,45943	2,32193	0,00000	0,00000	1,00000
HHIP	2,58496	4,32193	4,16993	1,00000	3,45943	3,32193	0,00000	0,00000	0,00000	0,00000
CNTN1	4,70044	3,45943	4,52356	3,00000	2,80735	0,00000	2,00000	0,00000	1,00000	2,32193
CNTNAP2	2,80735	3,16993	3,80735	3,32193	3,32193	0,00000	0,00000	0,00000	0,00000	2,58496
COL4A1	5,42626	4,08746	3,32193	5,12928	2,80735	2,32193	0,00000	0,00000	0,00000	1,58496
SLC6A12	4,70044	3,45943	5,24793	3,00000	1,58496	1,00000	1,00000	1,00000	4,24793	0,00000
PTGER2	3,16993	3,80735	3,70044	3,45943	0,00000	0,00000	0,00000	0,00000	2,80735	1,00000
NEURL2	2,32193	3,80735	2,32193	2,58496	2,58496	2,32193	1,00000	0,00000	0,00000	0,00000
BRSK2	2,58496	3,00000	2,00000	2,00000	2,32193	1,00000	2,00000	0,00000	0,00000	0,00000
FBLL1	2,00000	4,52356	0,00000	1,58496	2,00000	0,00000	1,00000	1,00000	0,00000	0,00000
DIO1	2,00000	5,16993	2,32193	2,00000	0,00000	0,00000	1,00000	0,00000	0,00000	0,00000
KLHL14	1,00000	2,58496	2,32193	2,00000	0,00000	0,00000	0,00000	0,00000	0,00000	0,00000
SULT4A1	4,70044	1,58496	0,00000	4,24793	0,00000	0,00000	0,00000	0,00000	1,00000	0,00000
LUM	5,49185	2,32193	0,00000	2,32193	0,00000	0,00000	0,00000	0,00000	0,00000	0,00000
UCHL1	3,16993	1,00000	1,00000	3,45943	1,00000	0,00000	0,00000	0,00000	0,00000	1,00000
PALMD	2,32193	2,32193	1,00000	3,90689	0,00000	0,00000	0,00000	0,00000	0,00000	0,00000
CES4A	3,16993	3,80735	2,00000	3,32193	3,00000	1,00000	0,00000	1,00000	0,00000	1,00000
AC022498.1	2,32193	3,32193	1,00000	3,80735	2,58496	0,00000	0,00000	1,58496	0,00000	1,00000
CELSR3	3,70044	3,45943	2,32193	2,80735	3,16993	0,00000	0,00000	3,58496	0,00000	1,58496
SCUBE2	2,58496	3,58496	4,16993	4,70044	0,00000	1,00000	0,00000	3,32193	0,00000	0,00000
CCDC74A	4,24793	4,24793	4,75489	4,08746	5,00000	0,00000	2,00000	2,32193	0,00000	3,58496
HPDL	4,39232	3,90689	4,70044	3,70044	4,08746	0,00000	1,00000	2,00000	0,00000	3,00000
TM6SF2	3,32193	4,24793	4,52356	2,58496	4,70044	0,00000	2,58496	3,00000	0,00000	3,45943
CYP1A1	3,16993	3,80735	5,88264	2,00000	4,24793	0,00000	1,00000	0,00000	0,00000	5,16993
TMEM253	3,00000	3,45943	5,32193	3,70044	4,90689	0,00000	2,32193	1,58496	3,45943	4,08746
PAH	1,58496	5,00000	5,95420	3,32193	6,53916	2,00000	1,00000	4,08746	3,00000	2,58496
GKN2	3,90689	7,11894	3,16993	1,58496	7,52356	1,58496	1,00000	3,32193	0,00000	3,32193
HEPH	7,56986	6,53916	8,65821	4,80735	6,28540	0,00000	2,80735	2,58496	1,00000	6,39232
IL1R2	5,42626	4,32193	6,56986	5,61471	5,42626	4,00000	2,80735	3,90689	2,80735	4,39232
GPA33	4,39232	5,24793	6,26679	6,00000	6,18982	2,58496	2,32193	3,58496	2,80735	4,80735
CAPN9	5,12928	3,45943	5,67243	5,04439	6,88264	2,80735	3,32193	5,61471	4,16993	2,32193
PRODH	4,85798	2,58496	6,80735	6,83289	7,58496	5,16993	1,00000	5,49185	3,70044	4,32193
FAM211A	5,00000	3,90689	6,28540	4,90689	4,08746	3,70044	0,00000	0,00000	4,52356	3,80735
MMP24	4,70044	3,45943	4,95420	6,65821	2,00000	2,00000	1,00000	3,58496	4,16993	3,45943
IRF8	2,00000	6,79442	6,04439	4,24793	0,00000	3,00000	2,58496	0,00000	0,00000	1,58496
SLC6A19	0,00000	4,08746	7,52356	5,61471	2,00000	1,00000	2,00000	0,00000	0,00000	0,00000
MUC6	0,00000	7,42626	8,71768	4,95420	0,00000	4,32193	0,00000	2,32193	2,00000	0,00000
SYNE1	3,16993	1,00000	3,00000	1,00000	0,00000	5,20945	3,16993	3,00000	3,58496	2,80735
ZIK1	2,00000	1,58496	2,00000	0,00000	0,00000	4,08746	2,58496	2,80735	5,35755	3,16993
IL2RG	1,00000	2,58496	3,32193	0,00000	1,58496	5,20945	3,58496	3,16993	2,80735	2,58496
IFITM1	2,32193	1,58496	0,00000	0,00000	0,00000	5,49185	2,32193	3,00000	4,95420	1,00000
GNA15	1,00000	2,32193	0,00000	0,00000	1,00000	4,00000	2,00000	4,39232	3,45943	2,32193
CCNA1	0,00000	0,00000	1,00000	1,00000	0,00000	6,08746	3,32193	4,24793	3,45943	1,58496
ICAM1	2,00000	1,00000	0,00000	0,00000	3,80735	5,97728	4,08746	3,16993	3,16993	3,32193
C21orf67	2,00000	0,00000	0,00000	0,00000	1,58496	4,85798	2,00000	3,32193	0,00000	3,16993
C6orf100	2,58496	1,00000	0,00000	1,58496	1,00000	4,08746	4,52356	1,58496	3,00000	1,58496
CDH5	0,00000	0,00000	0,00000	0,00000	0,00000	5,49185	3,90689	0,00000	3,16993	2,32193
SLC16A14	1,58496	0,00000	0,00000	0,00000	1,58496	4,90689	2,00000	3,00000	3,00000	0,00000
NKAPL	1,00000	0,00000	0,00000	0,00000	2,00000	3,90689	1,00000	3,32193	3,00000	1,58496
RP11-297N6.4	0,00000	1,00000	0,00000	0,00000	0,00000	3,70044	0,00000	1,58496	3,90689	1,00000
AKT3	0,00000	0,00000	0,00000	0,00000	0,00000	3,00000	0,00000	1,00000	4,16993	0,00000

CALCB	0,00000	0,00000	0,00000	0,00000	0,00000	4,32193	1,00000	0,00000	2,80735	1,00000
S100A9	0,00000	0,00000	0,00000	0,00000	0,00000	5,00000	2,32193	1,00000	1,00000	0,00000
GATA2	0,00000	0,00000	0,00000	0,00000	0,00000	2,58496	2,00000	1,58496	1,00000	0,00000
SYT5	1,00000	1,00000	0,00000	1,00000	0,00000	2,80735	2,00000	2,58496	2,00000	2,32193
LRRC48	1,00000	0,00000	0,00000	0,00000	0,00000	1,00000	2,00000	1,58496	3,16993	2,00000
HLA-DRA	0,00000	2,00000	0,00000	0,00000	0,00000	4,16993	0,00000	2,80735	5,49185	0,00000
CDKL1	1,58496	2,32193	1,00000	2,32193	1,00000	3,80735	3,32193	2,00000	3,58496	4,08746
MT1G	0,00000	3,00000	0,00000	2,32193	1,58496	3,45943	2,58496	2,32193	4,58496	4,16993
SOX8	1,58496	3,45943	0,00000	1,00000	1,58496	2,00000	2,80735	5,00000	5,35755	3,80735
GABRB3	2,00000	3,45943	1,00000	0,00000	3,90689	3,32193	5,32193	1,00000	4,95420	6,06609
DHRS2	1,00000	1,58496	2,00000	0,00000	3,70044	0,00000	4,24793	3,58496	5,12928	6,40939
ST8SIA6	0,00000	0,00000	0,00000	1,58496	1,00000	0,00000	4,39232	3,80735	4,45943	3,00000
ZFP57	0,00000	0,00000	0,00000	0,00000	0,00000	0,00000	4,95420	3,45943	5,83289	2,32193
SERPINB2	2,32193	1,00000	0,00000	2,58496	4,00000	5,72792	3,32193	1,00000	0,00000	7,39232
CORO1A	2,58496	0,00000	0,00000	3,90689	2,58496	8,31288	4,85798	4,95420	5,24793	5,52356
TMEM173	4,08746	0,00000	0,00000	1,58496	2,00000	6,45943	5,45943	5,16993	5,12928	4,16993
MLF1	3,45943	1,00000	2,00000	3,32193	2,00000	5,83289	3,32193	5,45943	5,67243	5,55459
FLI1	0,00000	1,58496	0,00000	4,16993	3,45943	4,80735	5,85798	4,32193	4,32193	4,95420
DUSP10	4,08746	1,58496	0,00000	2,00000	1,58496	5,20945	4,39232	4,08746	2,32193	4,08746
ADAMTS14	3,32193	1,00000	0,00000	2,58496	1,00000	5,42626	3,90689	4,08746	4,00000	3,70044
CPE	3,80735	0,00000	0,00000	1,00000	0,00000	3,80735	3,80735	4,90689	2,00000	3,45943
IQCG	3,00000	1,00000	0,00000	3,00000	2,00000	2,58496	3,58496	4,64386	3,90689	4,32193
TCF15	2,58496	1,00000	3,32193	2,00000	2,58496	4,90689	4,39232	4,58496	2,00000	6,14975
DCLK1	1,58496	3,00000	1,00000	3,32193	2,32193	7,22882	4,08746	3,70044	2,80735	3,32193
CELF2	0,00000	3,16993	0,00000	1,58496	2,00000	7,15987	3,58496	4,95420	2,80735	1,58496
IGFL1	2,80735	2,58496	2,32193	2,80735	0,00000	6,52356	3,90689	3,90689	4,90689	0,00000
FOSB	2,80735	3,80735	0,00000	1,00000	1,58496	5,67243	6,89482	8,98584	0,00000	0,00000
HLA-DQB1	5,12928	1,00000	0,00000	0,00000	5,88264	0,00000	0,00000	8,83920	7,97728	6,33985
AC174470.1	7,37504	6,71425	7,73471	7,45121	6,83289	10,18239	7,69349	7,84549	9,09011	9,18735
FAM195B	7,37504	6,68650	7,65821	7,39232	6,83289	10,17866	7,57743	7,83920	9,07146	9,17243
CDKN2A	7,29462	6,87036	8,43045	8,05528	8,11374	10,38802	7,54689	7,27612	9,28309	9,33539
HYAL2	8,33985	8,11894	8,88570	7,90689	8,11374	10,97011	7,95420	8,64746	8,93958	9,30150
KRT16	8,18488	8,17493	7,78790	8,63300	8,29921	10,24436	7,15987	9,21432	8,97441	9,46964
SH3BP5L	7,47573	7,42626	7,19967	6,98868	9,52552	10,10460	7,30378	9,04439	7,78790	10,08082
PRMT1	7,60733	7,35755	7,83289	6,75489	8,60363	10,01262	7,33092	7,98868	8,33092	9,16491
CTD-3214H19.16	7,65105	7,71425	8,36194	7,52356	7,45943	9,23840	8,34873	8,14466	9,58120	8,74819
TRAPPC5	7,65105	7,71425	8,36194	7,52356	7,45943	9,23840	8,34873	8,14466	9,58120	8,74819
DPCD	7,96578	7,92481	7,83289	7,89482	7,55459	8,83920	8,31288	8,31741	10,79279	7,96000
C8orf59	7,01123	7,47573	7,10852	7,82018	8,07682	8,72451	7,95420	7,40939	10,04166	8,25267
APLP1	8,08746	7,04439	8,56986	6,79442	7,78790	9,15987	8,35755	9,41574	9,31288	7,80735
MT2A	6,47573	6,52356	7,62205	7,01123	5,70044	9,94251	8,72110	9,06609	9,98014	8,22882
SERTAD1	7,34873	6,91886	6,91886	6,75489	7,09803	8,12928	8,00562	7,97728	8,23840	8,37069
MGMT	6,33985	6,87036	6,26679	7,07682	7,17991	8,68650	7,29462	7,53138	8,58871	7,55459
GALK1	5,52356	7,33985	7,15987	6,68650	7,53138	8,29462	8,09803	8,16491	8,13955	8,14466
ZG16B	6,37504	7,45121	7,49185	6,37504	6,26679	9,00843	8,03342	7,26679	8,78790	6,61471
OAZ2	6,93074	6,33985	6,55459	6,71425	7,79442	9,36194	7,00000	7,03342	7,15987	8,68650
CCDC124	6,32193	6,16993	6,61471	5,93074	7,40939	9,09803	6,00000	7,06609	7,13955	8,38802
TSSC4	6,78136	6,45943	7,54689	6,79442	7,84549	9,36194	6,47573	6,94251	8,51570	8,93074
STMN2	7,01123	5,58496	3,80735	6,82018	5,08746	9,25974	8,54303	10,04029	9,98014	9,76155
APOL1	8,75154	8,31741	8,92778	9,01123	9,85175	9,78627	10,42417	10,88417	10,36960	9,86882
JUN	8,22882	8,99435	8,98584	9,07682	8,89482	9,73640	9,44915	11,39714	8,69697	9,02514
IFITM2	9,21432	7,53138	10,24079	7,80090	8,35315	10,87958	9,87652	10,55075	10,34983	8,56605
TSPAN13	8,45533	9,03342	8,35755	8,83289	9,28771	9,29002	9,95565	8,53916	11,88874	9,02514
RNASET2	8,82018	8,17493	8,39232	7,80090	8,53138	9,82337	10,35094	9,62022	9,75822	7,36632
EGR1	8,54303	8,27612	7,87036	8,55459	8,01681	7,94251	10,10591	10,91214	8,84235	7,45943
SDF2L1	8,31741	7,85175	8,40939	8,87958	9,58496	10,49685	8,14975	8,69349	9,02237	11,64746
U2AF2	7,77479	8,03342	8,54689	7,83920	10,20823	11,29175	7,83289	8,85487	8,54303	11,13443
HNRNPA0	9,13699	9,08746	9,37504	8,87652	9,70044	9,80574	8,96000	9,26444	8,98299	13,91308
SLC7A7	9,16491	8,70736	9,33985	9,22641	8,92778	5,70044	7,79442	8,52748	6,33985	8,64746
B3GALT5	9,72281	8,60363	8,83605	8,65105	9,11634	5,55459	8,33539	7,53916	6,78136	8,81057
LOXL4	9,80896	8,62571	9,45943	9,94105	7,67243	7,67948	8,58120	8,30834	8,33539	8,29462
FKBP11	9,31515	9,43671	9,12928	8,48784	8,23362	7,92481	7,39232	7,72110	7,96000	7,53138
ANO1	8,85487	9,21432	9,14720	8,82337	8,63662	7,63662	7,34873	7,82018	7,55459	7,88874

S100A4	9,21432	9,23601	9,17742	7,62205	8,70736	8,36632	6,79442	7,12928	7,40939	8,13955
CAPN8	8,52356	9,73132	8,94544	8,88264	8,92481	6,44294	8,73132	7,72110	7,59991	6,89482
IMPA2	7,75489	8,54689	8,98868	8,29462	8,77808	6,10852	7,79442	7,20945	7,51570	7,44294
CA12	7,67243	9,33762	8,92481	7,75489	7,69349	7,37504	7,27612	7,70044	7,98299	6,37504
SLC43A1	6,44294	8,45533	8,51964	9,03342	8,92481	6,40939	7,61471	8,25739	6,93074	6,74147
ACSS1	7,98868	8,75489	8,24793	7,82018	8,51570	6,04439	7,78136	6,16993	6,83289	6,02237
C2orf72	8,81378	7,83289	8,67243	7,89482	6,75489	5,32193	7,71425	7,06609	6,70044	6,58496
SYT8	8,16993	9,43045	9,98014	7,20945	8,82972	7,33092	6,40939	5,08746	9,15482	7,08746
MYEOV	9,54689	7,79442	9,43879	8,93664	7,93664	7,03342	7,30378	3,80735	6,78136	8,68299
TSKU	7,28540	7,60733	7,52356	7,22882	8,16491	6,37504	6,35755	7,14975	5,95420	6,75489
AUTS2	6,93074	7,97154	7,59246	7,56224	8,13955	5,90689	6,26679	7,00000	6,47573	6,45943
AC073610.5	7,69349	7,73471	7,68650	6,95420	6,79442	6,40939	5,80735	6,47573	6,62936	6,02237
ETV4	6,32193	6,87036	8,63662	7,02237	7,37504	6,88264	6,82018	6,18982	5,80735	6,04439
FAM198B	7,33092	5,78136	6,47573	6,44294	7,93664	6,12928	6,32193	5,45943	6,04439	5,67243
WSCD1	6,82018	7,30378	7,71425	8,47168	7,27612	5,58496	6,52356	5,97728	6,62936	6,94251
SIRPA	7,87652	6,39232	7,00000	9,03892	6,40939	5,42626	6,65821	5,42626	6,62936	6,32193
MYLK	8,68299	6,94251	7,08746	8,44294	5,97728	6,85798	6,06609	7,08746	6,06609	6,37504
TM4SF5	8,52748	7,85175	8,51570	8,84235	8,56605	6,16993	7,01123	7,39232	5,39232	7,43463
SLCO2B1	8,65105	7,85798	8,78136	7,65821	8,09803	5,75489	7,37504	5,75489	3,90689	7,94837
AMN	7,09803	8,08746	7,49185	7,84549	8,09803	4,95420	7,06609	7,11894	5,20945	5,85798
KLF2	7,28540	7,57743	6,89482	7,04439	8,61839	5,24793	6,40939	7,62205	3,58496	7,17991
LGALS1	7,20945	9,47371	8,28540	8,71425	7,29462	7,07682	8,82655	7,44294	5,72792	2,80735
NDRG4	10,90162	5,24793	7,67948	8,62936	5,24793	5,67243	8,05528	6,74147	6,47573	6,68650
CNOT1	8,78463	9,04166	9,24793	13,58942	9,53722	8,04439	9,09540	9,31967	8,43045	9,25974
AKR1B10	7,85175	9,53528	9,76818	10,40195	11,10525	7,00000	8,22882	7,61471	7,26679	9,30150
GSTM4	9,92333	11,18177	10,62205	10,30720	9,55075	8,18488	9,67772	9,01681	7,37504	7,67948
CEACAM5	10,28656	10,47573	11,27146	8,59991	11,19106	4,80735	7,63662	8,96000	6,82018	9,28771
UGT1A1	10,89785	10,59898	8,30834	9,60733	9,67243	4,32193	8,15987	6,16993	6,52356	8,95710
ALDH3A1	7,09803	12,01959	10,66000	7,47573	12,86438	7,97728	7,28540	7,10852	8,25267	9,68124
PCK1	7,75489	11,52209	10,22521	7,65105	11,08547	7,29462	10,24793	7,70044	7,12928	6,30378
DPCR1	8,47168	10,89026	7,12928	7,97154	11,01890	6,78136	4,52356	7,00000	4,24793	8,93074
PSCA	9,43879	11,98335	6,80735	7,27612	6,79442	4,39232	6,56986	10,24079	6,18982	6,61471
RPS5	10,67507	10,84392	11,60548	10,66000	11,39767	13,20105	11,49085	11,42522	12,70304	12,51274
RPL18A	9,94398	10,48884	11,18549	10,35975	10,75405	11,56415	10,82416	12,29290	11,86225	11,17617
ADAM15	9,52943	9,62022	10,14720	9,16491	11,51274	12,87094	10,13057	11,44139	10,36741	11,56367
KLK10	12,14179	10,93884	9,13443	8,96578	11,55794	13,34207	9,82337	12,63095	12,43593	11,03136
RPL6	9,83920	9,69870	9,69349	9,85953	9,79116	10,17742	10,29232	12,35590	10,22762	10,39124
SPINK1	9,51964	9,40088	8,20457	9,30606	11,12412	9,27845	11,47523	12,27088	11,25267	10,34319
SLC2A3	10,45635	8,80413	9,72622	10,22038	8,27146	11,66800	11,31232	10,97370	10,28077	11,05053
TIMP2	12,11927	9,80252	11,01193	10,80977	9,21432	10,03617	10,15861	9,91139	9,51570	9,97871
SPINK4	11,21614	11,16554	12,14530	10,47675	10,10591	8,58120	7,92481	9,84078	10,42206	10,34096
MUC5AC	10,90989	11,66133	12,89936	12,18239	12,83881	10,79523	8,22882	11,12606	9,99718	9,51175
MMP1	12,31430	14,04226	13,28179	13,26766	12,95529	9,40514	11,87114	11,45584	13,47649	12,52674
REG4	12,86728	12,55746	14,61442	13,81328	13,55315	10,21675	10,57270	10,93295	11,28829	13,51138
AQP3	11,84667	13,97719	13,62970	11,16993	11,15987	11,07548	11,19353	10,09408	12,59898	11,31515
TFF2	10,88188	12,86225	12,33260	11,27903	12,83249	10,51274	10,82893	10,09144	11,45892	11,88798
CYSTM1	13,31288	13,33497	13,99789	13,29247	13,24377	11,71596	12,99894	12,51274	12,49685	11,97298
TFF1	11,79360	13,98789	13,21796	13,47485	14,92152	11,68475	13,01924	13,00440	12,10263	12,88760
RPS9	11,80574	11,69957	12,42495	11,30435	12,54352	14,43313	11,90651	12,48003	12,79726	13,09358

Table S3: Genecodis analysis

GO biological process

all signature genes

Genes	NGR	TNGR	NG	TNG	Hyp	Hyp*	Annotations
13 genes	136	34208	13	341	0,000123	0,124843	GO:0006805: xenobiotic metabolic process (BP)
9 genes	56	34208	9	341	0,000439	0,222782	GO:0007586: digestion (BP)
24 genes	630	34208	24	341	0,002805	0,948987	GO:0055085: transmembrane transport (BP)
13 genes	181	34208	13	341	0,003935	0,998436	GO:0019221: cytokine-mediated signaling pathway (BP)
20 genes	549	34208	20	341	0,082354	0.0001671	GO:0006811: ion transport (BP)
30 genes	1176	34208	30	341	0,299356	0.0005064	GO:0007165: signal transduction (BP)
7 genes	75	34208	7	341	1,02096	0.0012953	GO:0060337: type I interferon-mediated signaling pathway (BP)
9 genes	136	34208	9	341	0,965131	0.0013994	GO:0032496: response to lipopolysaccharide (BP)
3 genes	6	34208	3	341	1,92057	0.0021659	GO:0046483: heterocycle metabolic process (BP)
7 genes	88	34208	7	341	2,92364	0.0029675	GO:0008202: steroid metabolic process (BP)

downregulated signature genes

Genes	NGR	TNGR	NG	TNG	Hyp	Hyp*	Annotations
12 genes	136	34208	12	225	1,21E-05	0,004089	GO:0006805: xenobiotic metabolic process (BP)
9 genes	56	34208	9	225	1,14E-05	0,007686	GO:0007586: digestion (BP)
21 genes	630	34208	21	225	0,00015	0,033903	GO:0055085: transmembrane transport (BP)
19 genes	549	34208	19	225	0,000513	0,086713	GO:0006811: ion transport (BP)
7 genes	88	34208	7	225	0,195953	0.0002649	GO:0008202: steroid metabolic process (BP)
3 genes	6	34208	3	225	0,553433	0.0006235	GO:0046483: heterocycle metabolic process (BP)
4 genes	20	34208	4	225	0,081281	0.0006868	GO:0017144: drug metabolic process (BP)
5 genes	41	34208	5	225	0,727521	0.0007025	GO:0006865: amino acid transport (BP)
2 genes	2	34208	2	225	4,30713	0.0032351	GO:0046485: ether lipid metabolic process (BP)
8 genes	200	34208	8	225	5,77955	0.0039069	GO:0034641: cellular nitrogen compound metabolic process (BP)

upregulated signature genes

Genes	NGR	TNGR	NG	TNG	Hyp	Hyp*	Annotations
7 genes	181	34208	7	116	0,296553	0.0015450	GO:0019221: cytokine-mediated signaling pathway (BP)
8 genes	341	34208	8	116	2,24209	0.0058406	GO:0008285: negative regulation of cell proliferation (BP)
14 genes	1176	34208	14	116	4,62423	0.0080307	GO:0007165: signal transduction (BP)
3 genes	23	34208	3	116	6,40348	0.0083405	GO:0002504: antigen processing and presentation of peptide or polysaccharide antigen via MHC class II (BP)
5 genes	136	34208	5	116	0.0001038	0.0108246	GO:0032496: response to lipopolysaccharide (BP)
4 genes	93	34208	4	116	0.0002904	0.0116398	GO:0006414: translational elongation (BP)
4 genes	82	34208	4	116	0.0001790	0.0116601	GO:0060333: interferon-gamma-mediated signaling pathway (BP)
4 genes	82	34208	4	116	0.0001790	0.0116601	GO:0019083: viral transcription (BP)
4 genes	92	34208	4	116	0.0002786	0.0120989	GO:0045471: response to ethanol (BP)
2 genes	7	34208	2	116	0.0002367	0.0123351	GO:0019886: antigen processing and presentation of exogenous peptide antigen via MHC class II (BP)

KEGG pathways

all signature genes

Genes	NGR	TNGR	NG	TNG	Hyp	Hyp*	Annotations
11 genes	68	34208	11	341	7,6E-06	0,001102	(KEGG) 00980: Metabolism of xenobiotics by cytochrome P450
9 genes	70	34208	9	341	0,003334	0,024172	(KEGG) 00982: Drug metabolism - cytochrome P450
7 genes	61	34208	7	341	0,252841	0.0001222	(KEGG) 00830: Retinol metabolism
6 genes	52	34208	6	341	1,29913	0.0004709	(KEGG) 00140: Steroid hormone biosynthesis
4 genes	26	34208	4	341	0.0001219	0.0035366	(KEGG) 00053: Ascorbate and aldarate metabolism
6 genes	84	34208	6	341	0.0001985	0.0035992	(KEGG) 05323: Rheumatoid arthritis
5 genes	51	34208	5	341	0.0001541	0.0037253	(KEGG) 04978: Mineral absorption
4 genes	29	34208	4	341	0.0001892	0.0039198	(KEGG) 00591: Linoleic acid metabolism
7 genes	125	34208	7	341	0.0002683	0.0043236	(KEGG) 04514: Cell adhesion molecules (CAMs)
8 genes	172	34208	8	341	0.0003515	0.0050971	(KEGG) 05152: Tuberculosis

downregulated signature genes

Genes	NGR	TNGR	NG	TNG	Hyp	Hyp*	Annotations
9 genes	68	34208	9	225	6,91E-05	0,000705	(KEGG) 00980: Metabolism of xenobiotics by cytochrome P450
7 genes	70	34208	7	225	0,040902	2,08599	(KEGG) 00982: Drug metabolism - cytochrome P450
4 genes	29	34208	4	225	3,80365	0.0012932	(KEGG) 00591: Linoleic acid metabolism
5 genes	61	34208	5	225	5,19025	0.0013235	(KEGG) 00830: Retinol metabolism
3 genes	23	34208	3	225	0.0004511	0.0076700	(KEGG) 00910: Nitrogen metabolism
4 genes	52	34208	4	225	0.0003851	0.0078574	(KEGG) 00140: Steroid hormone biosynthesis
4 genes	62	34208	4	225	0.0007539	0.0109867	(KEGG) 00010: Glycolysis / Gluconeogenesis
4 genes	70	34208	4	225	0.0011895	0.0151669	(KEGG) 03320: PPAR signaling pathway
3 genes	39	34208	3	225	0.0021548	0.0244212	(KEGG) 00620: Pyruvate metabolism
3 genes	53	34208	3	225	0.0051633	0.0438887	(KEGG) 00590: Arachidonic acid metabolism

upregulated signature genes

Genes	NGR	TNGR	NG	TNG	Hyp	Hyp*	Annotations
6 genes	172	34208	6	116	2,78101	0.0026697	(KEGG) 05152: Tuberculosis
4 genes	66	34208	4	116	7,69183	0.0036920	(KEGG) 05140: Leishmaniasis
4 genes	86	34208	4	116	0.0002151	0.0041303	(KEGG) 03010: Ribosome
3 genes	34	34208	3	116	0.0002105	0.0050534	(KEGG) 04940: Type I diabetes mellitus
3 genes	46	34208	3	116	0.0005185	0.0055313	(KEGG) 05150: Staphylococcus aureus infection
4 genes	102	34208	4	116	0.0004129	0.0056631	(KEGG) 05142: Chagas disease (American trypanosomiasis)
3 genes	45	34208	3	116	0.0004859	0.0058312	(KEGG) 00514: Other types of O-glycan biosynthesis
4 genes	113	34208	4	116	0.0006080	0.0058371	(KEGG) 04670: Leukocyte transendothelial migration
4 genes	84	34208	4	116	0.0001964	0.0062875	(KEGG) 05323: Rheumatoid arthritis
4 genes	101	34208	4	116	0.0003977	0.0063644	(KEGG) 04620: Toll-like receptor signaling pathway

NGR = Number of annotated genes in the reference list;
TNGR = Total number of genes in the reference list;
NG = Number of annotated genes in the input list;
TNG = Total number of genes in the input list;
Hyp = Hypergeometric pValue; Hyp* = Corrected hypergeometric pValue

Tabas-Madrid D, Nogales-Cadenas R, Pascual-Montano A: GeneCodis3: a non-redundant and modular enrichment analysis tool for functional genomics.
Nucleic Acids Research 2012; doi: 10.1093/nar/gks402
Nogales-Cadenas R, Carmona-Saez P, Vazquez M, Vicente C, Yang X, Tirado F, Carazo JM, Pascual-Montano A:
GeneCodis: interpreting gene lists through enrichment analysis and integration of diverse biological information. Nucleic Acids Research 2009; doi: 10.1093/nar/gkp416
Carmona-Saez P, Chagoyen M, Tirado F, Carazo JM, Pascual-Montano A: GENECODIS: A web-based tool for finding significant concurrent annotations in gene lists.
Genome Biology 2007 8(1):R3